UNIVERSITÀ DEGLI STUDI DI PARMA

Dottorato di Ricerca in Tecnologie dell'Informazione

XXVIII Ciclo

ADVANCED RECEIVERS FOR NEXT GENERATION WIRELESS COMMUNICATION SYSTEMS

Coordinatore:

Chiar.mo Prof. Marco Locatelli

Relatore:

Chiar.mo Prof. Gianluigi Ferrari

Tutor:

Chiar.mo Dr. Marco Martalò

Dottorando: *Muhammad Asim*

Gennaio 2016

To my family

Contents

List of Figures

Summary

Despite extensive progress on the theoretical aspects of spectral efficient communication systems, hardware impairments, such as phase noise, are the key bottlenecks in next generation wireless communication systems. The presence of non-ideal oscillators at the transceiver introduces time varying phase noise and degrades the performance of the communication system. Significant research literature focuses on joint synchronization and decoding based on joint posterior distribution, which incorporate both the channel and code graph. These joint synchronization and decoding approaches operate on well designed sum-product algorithms, which involves calculating probabilistic messages iteratively passed between the channel statistical information and decoding information. Channel statistical information, generally entails a high computational complexity because its probabilistic model may involve continuous random variables. The detailed knowledge about the channel statistics for these algorithms make them an inadequate choice for real world applications due to power and computational limitations.

In this thesis, novel phase estimation strategies are proposed, in which soft decision-directed iterative receivers for a separate A Posteriori Probability (APP)-based synchronization and decoding are proposed. These algorithms do not require any a priori statistical characterization of the phase noise process. The proposed approach relies on a Maximum A Posteriori (MAP)-based algorithm to perform phase noise estimation and does not depend on the considered modulation/coding scheme as it only exploits the APPs of the transmitted symbols. Different variants of APP-based phase estimation are considered. The proposed algorithm has significantly lower computa-

tional complexity with respect to joint synchronization/decoding approaches at the cost of slight performance degradation.

With the aim to improve the robustness of the iterative receiver, we derive a new system model for an oversampled (more than one sample per symbol interval) phase noise channel. We extend the separate APP-based synchronization and decoding algorithm to a multi-sample receiver, which exploits the received information from the channel by exchanging the information in an iterative fashion to achieve robust convergence. Two algorithms based on sliding block-wise processing with soft ISI cancellation and detection are proposed, based on the use of reliable information from the channel decoder.

Dually polarized systems provide a cost-and spatial-effective solution to increase spectral efficiency and are competitive candidates for next generation wireless communication systems. A novel soft decision-directed iterative receiver, for separate APP-based synchronization and decoding, is proposed. This algorithm relies on an Minimum Mean Square Error (MMSE)-based cancellation of the cross polarization interference (XPI) followed by phase estimation on the polarization of interest. This iterative receiver structure is motivated from Master/Slave Phase Estimation (M/S-PE), where M-PE corresponds to the polarization of interest. The operational principle of a M/S-PE block is to improve the phase tracking performance of both polarization branches: more precisely, the M-PE block tracks the co-polar phase and the S-PE block reduces the residual phase error on the cross-polar branch. Two variants of MMSE-based phase estimation are considered; BW and PLP.

Chapter 1

Introduction

The aim of this chapter is to present a general overview on the problems underlying the communication systems to achieve higher spectral efficiency for the next generation wireless communications systems. In particular, Section 1.1 motivates the scope of this thesis work, where Section 1.2 highlight the related work from the literature. Section 1.3 summarizes the aim of this thesis and Section 1.4 gives a brief overview of the following chapters.

1.1 Motivation

Wireless communication has witnessed tremendous advancement during the last few decades. Overwhelming data rates due to the emergence of broadband application service like video streaming and massive number of users such as smart phones, tablets and various types of machine-to-machine communication services, etc. This increasing demand with reliable communication plays an essential role in pushing this advancement for more spectrum efficient wireless communication systems in its next generations.

Despite extensive progress on the theoretical aspects of spectral efficient communication systems, the hardware impairments in radio-frequency and optical communications are the key bottlenecks of the performance. Power amplifier non-linearities,

channel non-linearities, oscillator phase noise, I/Q imbalance, sampling-rate and carrier frequency offsets are commonly known hardware impairments in wireless / optical transceiver. Different compensation schemes are typically applied to limit the impact of each of these impairments. However, in practice the compensation and calibration will not be perfect and residual noise from hardware impairments will still remain and have greater impact on the system performance and, therefore, should be taken into account. The advent of high performance digital signal processing helped to minimize the effects of hardware impairments. Appropriate mathematical models that can accurately represent the physical impairments are used to summarize the impact of unwanted effects into a communication channel.

Oscillator phase noise can be regarded among the key noise impairments, which severely limits the spectral efficiency of the digital communication system. The presence of non-ideal oscillators at the transceiver introduces time varying phase noise. A realistic oscillator is subject to unwanted noise, in terms of temporal instabilities and spectral dispersions. These instabilities, collectively referred to as phase noise [1], induce distortions (in the limiting case, complete loss of information) in traditional receivers.

The performance of lower-to-higher-order modulations, which employ dense constellations, are severely affected by phase noise and this is a limiting factor in high data rate digital communication systems. In addition to lower-to-higher-order modulations, the negative impact of the phase noise is more pronounced in different transmission schemes, which offer spectral efficient wireless communications. As an example of spectral efficient system, antenna polarization diversity offer a cost- and spatial-effective solution by transmitting two independent data streams through orthogonal polarizations using same carrier frequency [2, 3], where phase noise becomes detrimental and increases the cross polarization interference. The orthogonality of the subcarriers in orthogonal frequency division multiplexing (OFDM) systems is also affected by phase noise and results into an increase in inter-carrier interference [4, 5]. The performance of multiple antenna, such as Multiple Input Multiple output (MIMO) radio systems [6–8] are limited by the presence of phase noise.

1.2 Related Work

In digital communication systems, Additive White Gaussian Noise (AWGN) channel with phase noise is a widely used model to capture imperfect carrier-phase. The use of high quality oscillator in the communication equipment increases its cost, it is often preferable to use inexpensive oscillator and compensate for the phase noise effects by means of digial signal processing. The study of phase noise-impaired communications is well established in the literature, in terms of both achievable information rate and design of practical receivers coping with this hindrance. From an information-theoretic perspective, the ultimate performance limits in the presence of phase noise have been investigated under different channel models, see, e.g., [9–12] and references therein.

Several novel phase noise estimation techniques are proposed in the literature to enhanced the receiver performance in the presence of phase noise. Traditional approaches to combat phase noise are based on conventional feedback tracking schemes [13, 14]. A most common example of feedback algorithm, which solve the phase ambiguity problem are based on Phase Locked Loop (PLL) [15, 16]. However, these algorithms are not appropriate for higher-order constellations due to the degradation in the phase error estimation and need longer acquisition periods for burst transmission.

The issue of iterative phase synchronization is particularly relevant when powerful error-correction code, such as turbo codes [17] and low-density parity check codes [18], are used, as they require accurate phase estimation at very low Signal-to-Noise Ratio (SNR). The problem of iterative detection/decoding of data symbols transmitted over an AWGN channel in the presence of phase uncertainty is addressed in [19], where an iterative Maximum Likelihood (ML) algorithm, embedded into an Expectation-Maximization (EM) receiver, is derived. In [20], the authors extend the ML synchronization problem by considering Data-Aided (DA), Non-Code-Aided (NCA), and iterative Code-Aided (CA) synchronizers, all leading to iterative Phase Locked Loop (PLL)-based schemes. In [21], the authors propose a model of the phase uncertainty which allows to devise a variational Bayesian detection algorithm.

In another approach, phase noise is assumed to be quasi- constant over an observation interval (block window) and a feedforward algorithm can be used to estimate the local time average of phase in each sub-intervals [22]. However, the length of the observation interval should be smaller to track the phase noise variation accurately, whereas it should be long enough to average out the impact of the channel noise. In [23–25], discrete cosine transform (DCT) based basis expansion model is used at the front-end for phase noise estimation from the known transmitted information and then an iterative receiver structure is devised to improve the estimation accuracy by using the soft-information. In addition to this, other novel phase noise estimation schemes can be found in the literature [26–31] and references therein.

Several algorithms for joint synchronization and decoding are performed, which provide near optimal performance by using well-known sum-product algorithm [32–35]. The sum-product algorithm uses a factor graph, which incorporates both the phase estimation portion and channel decoding portion. The sum-product algorithm involves calculating probabilistic messages iteratively passed between these two portions. The phase estimation portion generally require a high computational complexity because its probabilistic model involve continuous random variables. In [33], a Tikhonov parameterization of the probabilistic model is employed as good tradeoff between complexity and performance. In [36], an innovative approach for mixture dimension reduction for Tikhonov canonical models is presented, which keeps accuracy levels high with lower complexity compare to [33]. The detailed knowledge about the phase noise statistics requirement for these algorithms make them an inadequate choice for real world applications due to power and computational complexity constraints.

1.3 Aim of the thesis

In this thesis, phase noise estimation for spectrally efficient wireless communication systems is investigated. The main objective of this thesis is to devise novel synchronization/detection schemes for pragmatic receiver structure. Some important aspects of the proposed novel phase noise estimation strategies are listed below.

- The proposed algorithms do not require any a priori statistical characterization of the phase noise process.
- Novel soft-decision directed iterative receiver, for separate A Posteriori Probability (APP)-based synchronization and decoding is proposed.
- The proposed approach is general in the sense that it does not depend on the considered modulation/coding scheme as it only exploits the APPs of the transmitted (modulated) symbols.
- Since the assumption of constant phase over a given observation interval is contrary to the Bayesian estimation, an extended version, denoted as sliding window, is proposed.

1.4 Overview of the Thesis

The remainder of the thesis is organized as follows.

In Chapter 2, a novel phase noise estimation algorithm is presented. In Section 2.1, the system model used in this chapter is discussed in detail. Section 2.2 presents the novel soft-decision directed algorithm for phase noise estimation with optimal strategies used for enhancing the performance of the system. The proposed iterative synchronization/detection receiver structure is discussed in Section 2.3 and detail performance analysis of the proposed schemes are conducted in Section 2.4. Finally, Section 2.5 concludes the chapter.

In Chapter 3, phase synchronization problem in the presence of Inter-Symbol Interference (ISI) is considered. Details about a realistic system model are given in Section 3.2. Section 3.3 focuses on the proposed receiver, which uses the APPs-from the decoder for phase synchronization purpose. The corresponding iterative synchronization receiver structure is shown in Section 3.4. The performance analysis is presented in Section 3.5. Finally, Section 3.6 concludes the chapter.

The phase synchronization problem in dually-polarized communications is discussed in Chapter 4. In Section 4.2, the system model used for the dually-polarized system is presented. Section 4.3, provide the detail about the proposed MMSE-based

phase noise estimation algorithm. Section 4.4, an iterative receiver structure for the proposed strategy is discussed. Performance analysis is given in Section 4.5 and Section 4.6 concludes this chapter.

Chapter 2

Reduced Complexity Phase Synchronization

The accuracy of the oscillator has an important role in spectral efficient digital communication as carrier phase instabilities leads to a degradation in the overall system performance. In this chapter, a Maximum A Posteriori (MAP)-based phase noise estimation algorithm is presented. In order to optimize the performance of block-based Maximum Likelihood (ML) phase noise estimation, new strategies are also presented for optimizing the performance of the communication systems.

The rest of the chapter is structured as follows. In Section 2.1, we present the system model and discuss different ingredients of the transmitter in detail. In Section 2.2, the proposed MAP-based phase noise estimation algorithm and some extended approaches are presented. The proposed iterative synchronization/detection receiver structure is discussed in Section 2.3 and a detailed Performance analysis of the proposed scheme are presented in Section 2.4. Finally, the Section 2.5 concludes the chapter.

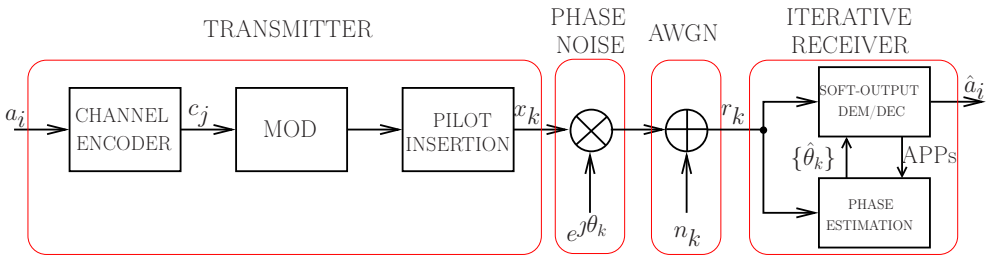

Figure 2.1: System model for phase noise impaired communications.

2.1 System Model

At the transmitter, the binary information sequence $\{a_i\}$ is generated at a bit rate equal to r_b bit/s. The information sequence $\{a_i\}$ is encoded into a sequence $\{c_j\}$ through a binary channel code with rate R. A modulation scheme with constellation size $M = 2^b$ and symbol energy E_s is then used.

2.1.1 Multi-Level Coding

In order to manage high-order modulation schemes, a multi-level channel encoding policy is considered [37]. For small-size constellations (say $b \leq b_1$, where b_1 is a small integer), all bits are encoded, whereas for medium/high-size constellations, i.e., for $b > b_1$, b_1 out of b bits are encoded and the remaining $b - b_1$ are left uncoded (free bits). This approach has the implementation advantage of keeping the coding strategy unaltered for modulations of various order. In this case, b_1 coded bits identify one of 2^{b_1} possible subsets of a constellation with 2^b points, whereas the $b - b_1$ free bits specify a given point of the selected subset. According to Ungerboeck set partitioning rules [13], subsets are designed so as to maximize the Euclidean distance using a set-partitioning [38]. Gray mapping, in terms of free bits, is used to label the points within a given subset [39, 40]. The overall spectral efficiency of the considered multi-level

coding scheme is

$$\eta = \begin{cases} R \cdot b \quad \text{bit/symb} & \text{if } b \leq b_1 \\ R \cdot b_1 + (b - b_1) \quad \text{bit/symb} & \text{if } b > b_1. \end{cases}$$

Although the proposed approach is very general (in terms of the considered coded modulation schemes) and, as it will be shown in Section 2.2, requires only APPs on the transmitted symbols. In particular, multi-level coding (with $b_1 = 4$) will be considered with a large constellation size (1024-QAM).

2.1.2 Pilot Symbols and Insertion Loss

Initial synchronization (in the absence of APPs) is performed through the insertion, in the transmitted frame, of pilot symbols known at the receiver [41]. We assume that N_p pilot symbols are interleaved every N data symbols, thus obtaining the following effective spectral efficiency:

$$\eta' = \eta \frac{N}{N + N_\mathrm{p}} \qquad \text{bit/symb.}$$

We also assume that each pilot symbol has energy E_p and define

$$q \triangleq \frac{N_\mathrm{p} E_\mathrm{p}}{N E_\mathrm{s}} \tag{2.1}$$

as the ratio between the pilot energy and the data symbol energy. The average data symbol energy can be expressed as

$$\overline{E}_\mathrm{s} = \frac{N_\mathrm{p} E_\mathrm{p} + N E_\mathrm{s}}{N} = E_\mathrm{s} (1 + q). \tag{2.2}$$

The factor $(1+q)$ is the energy penalty due to pilot symbol insertion. The utilization of pilot symbols at the receiver side will be detailed in Section 2.3.

The transmission channel introduces both AWGN and phase noise. For moderate phase dynamics [11], the received discrete-time equivalent baseband model shown in Figure 2.1 is

$$r_k = x_k e^{\theta_k} + n_k \qquad k = 1, 2, \ldots \tag{2.3}$$

where $\{x_k\}$ are the transmitted symbols and $\{n_k\}$ are independent and identically distributed (i.i.d.) Gaussian noise complex samples with per-component variance $\sigma^2 = N_0/2$. The average received energy per information bit is $\overline{E}_s/\eta$ and the per-bit Signal-to-Noise Ratio (SNR) γ_b can be finally defined as follows:

$$\gamma_b \triangleq \frac{E_b}{N_0} = \frac{\overline{E}_s}{N_0}\frac{1}{\eta} = \frac{E_s}{N_0}\frac{1+q}{\eta}. \tag{2.4}$$

Note that the considered system model in (2.3) is a memory-less channel model, where phase noise is introduced at the transmitted symbols and the channel assumes perfect channel state information i.e., the channel is free from any non-linearities such as Inter-symbol interference (ISI).

2.1.3 Phase Noise Model

The phase noise is modeled as a wiener process generated by integrating a white Gaussian process and characterize by its Power Spectral density (PSD) $2\pi B_\theta$. The discrete-time phase noise $\{\theta_k\}$ at the k-th instant in (2.3) can be described as first-order Markov, namely:

$$\theta_k = \theta_{k-1} + \Delta_k \mod 2\pi \tag{2.5}$$

where $\Delta_k \sim \mathcal{N}(0, \sigma_\Delta^2)$ and variance $\sigma_\Delta^2 = 2\pi B_\theta T$, where T describe the symbol interval and B_θ controls the intensity of the phase noise process. $B_\theta = 2\Delta f_{3dB}$, i.e., the frequency spacing between the 3-dB points of the Lorentzian PSD, where $\Delta f_{3dB} = \pi f_c^2 \alpha_{\text{osc}}$ [42]. α_{osc} determines the oscillator quality and has linear relationship with the σ_Δ^2 [43], where f_c is the carrier (oscillator) frequency. In practice, the constant α_{osc} is not directly available, instead a measure used to describe the oscillator performance is the decay of the oscillator PSD around the first harmonic $\mathscr{L}(f_o)$[dBc/Hz] [42], where f_o is the frequency offset with respect to the f_c. The connection between the $\mathscr{L}(f_o)$ and α_{osc} is achieved through the relation $\mathscr{L}(f_o) \approx 10log_{10}(\alpha_{\text{osc}} f_c^2/f_0^2)$, which holds for f_0 much larger than the phase noise 3-dB bandwidth denoted byΔf_{3dB}.

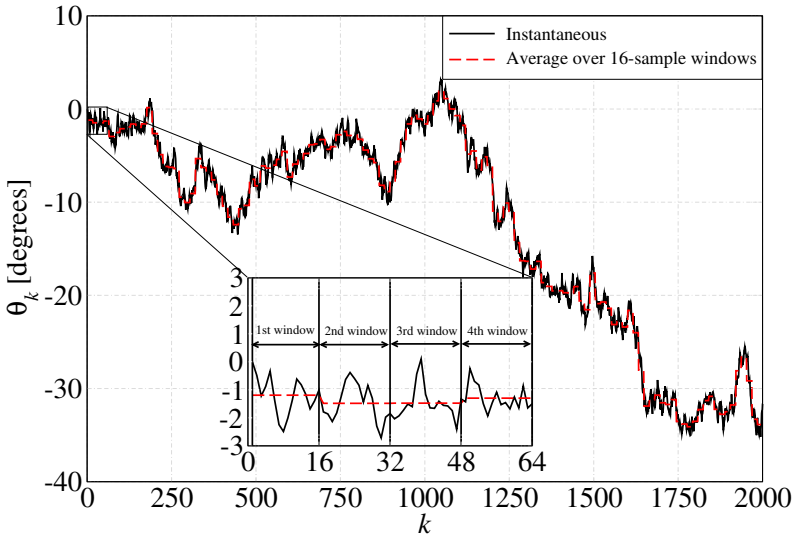

Figure 2.2: Example of a realization of the phase noise process for $\sigma_\Delta = 0.51^\circ$. For comparison, the average phase over a window of size 16 is also shown. In the inset, a zoom is shown for the first 16-symbol blocks.

2.2 MAP-based Phase Noise Estimation

We now describe a novel soft-decision aided iterative synchronization and decoding algorithm for an LDPC-coded communications over a phase noise-impaired channel. The soft information output by a channel decoder is used to perform a soft phase estimation, i.e., to estimate the channel phase based on the A-Posteriori Probability (APPs) of the transmitted symbols. This approach allows to properly weight the transmitted symbols in the phase estimation process: the more reliable the transmitted symbol, the more accurate the phase estimate.

2.2.1 Block Window

The key idea behind our algorithm is derived from [44], where the phase is assumed constant over the entire transmission frame, i.e., a phase offset is applied to the en-

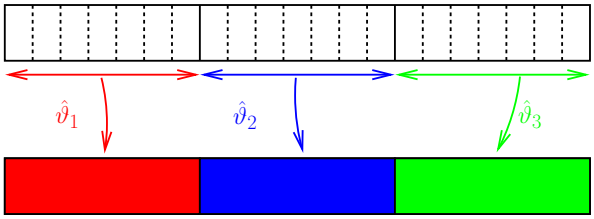

(a)

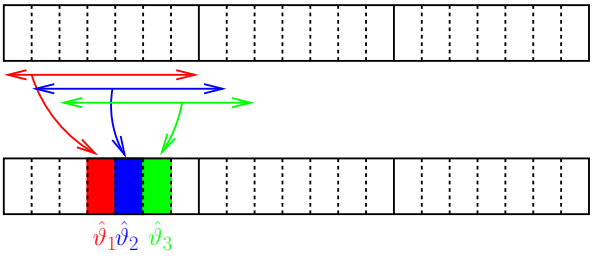

(b)

Figure 2.3: Window choices for the phase estimation algorithm: (a) block window (disjoint blocks), and (b) sliding window.

tire signal. In this work, we extend this idea by assuming that the channel phase can be considered constant over a (sufficiently short) observation period of ℓ consecutive samples. In Figure 2.2, an example of a realization of the phase noise process for $\sigma_\Delta = 0.51^\circ$ is shown. For comparison, the average phase over a window of 16 consecutive samples is also shown. From the inset, one can observe that the channel is severly impaired by the phase noise, with possible large deviations even during small time intervals. However, the correct phase value can be tracked by sufficiently short windows, according to the coherence time of the phase noise process.

We first focus on disjoint windows, i.e., the phase estimated for a block of length ℓ is used to derotate the symbols over the same block and is, in general, different from those estimated in adjacent blocks as shown in Figure. 2.3 (a). In other words, the estimated phase has a step-wise trend and referred to as Block Window (BW).

Consider a finite length-ℓ observation window

$$\boldsymbol{r}_k \triangleq [r_{k-\ell+1}, \ldots, r_k]$$

over which the phase is assumed to be constant. The ML phase estimate is

$$\hat{\theta}_k = \underset{\theta}{\operatorname{argmax}}\, p(\boldsymbol{r}_k|\theta) = \underset{\theta}{\operatorname{argmax}} \sum_{\boldsymbol{x}_k \in \mathscr{X}^\ell} p(\boldsymbol{r}_k|\theta, \boldsymbol{x}_k) P(\boldsymbol{x}_k)$$

where

$$\boldsymbol{x}_k \triangleq [x_{k-\ell+1}, \ldots, x_k]$$

and $\mathscr{X}$ denotes the set of possible QAM symbols. The ML estimate is equivalent to the maximum a-posteriori probability (MAP) strategy. In fact, using the Bayes rule one obtains

$$\begin{aligned} \hat{\theta}_k &= \underset{\theta}{\operatorname{argmax}}\, p(\theta|\boldsymbol{r}_k) \\ &= \underset{\theta}{\operatorname{argmax}}\, \frac{p(\boldsymbol{r}_k|\theta) p(\theta)}{p(\boldsymbol{r}_k)} \\ &= \underset{\theta}{\operatorname{argmax}}\, p(\boldsymbol{r}_k|\theta) \end{aligned}$$

since θ is uniformly distributed and $p(\boldsymbol{r}_k)$ is independent from θ.

Considering the available APPs as useful additional information, a modified ML strategy can be adopted:

$$\hat{\theta}_k \simeq \underset{\theta}{\operatorname{argmax}} \sum_{\boldsymbol{x}_k \in \mathscr{X}^\ell} \underbrace{p(\boldsymbol{r}_k|\theta, \boldsymbol{x}_k)}_{\text{Known}} \underbrace{P(\boldsymbol{x}_k|\boldsymbol{r})}_{\text{From LDPC dec.}}$$

where $\boldsymbol{r}$ is the entire collection of received samples over which the LDPC decoder works. In particular, the term $p(\boldsymbol{r}_k|\theta, \boldsymbol{x}_k)$ is known, from the channel model, to be a Gaussian pdf, whereas the terms $\{P(\boldsymbol{x}_k|\boldsymbol{r})\}$ can be obtained starting from the bit LLRs output by the channel decoder.

Let us assume independence between QAM symbols associated with a code block. This assumption is reasonable for interleaved convolutional codes and randomly generated LDPC codes. In the considered scenario, the use of structured LDPC

codes may hinder the validity of this assumption and the use of a bit interleaver can be investigated to improve the performance. Using independence, one obtains

$$\begin{aligned}
\hat{\theta}_k &\simeq \underset{\theta}{\operatorname{argmax}} \sum_{\boldsymbol{x}_k \in \mathscr{X}^\ell} \prod_{l=0}^{\ell-1} p(r_{k-l}|\theta, x_{k-l}) P(x_{k-l}|\boldsymbol{r}) && (2.6)\\
&= \underset{\theta}{\operatorname{argmax}} \prod_{l=0}^{\ell-1} \left[\sum_{m=0}^{M-1} p(r_{k-l}|\theta, x_{k-l}) p_{lm} \right] && (2.7)\\
&= \underset{\theta}{\operatorname{argmax}} \prod_{l=0}^{\ell-1} \left[\sum_{m=0}^{M-1} \frac{1}{2\pi\sigma^2} e^{-\frac{1}{2\sigma^2}\left| r_{k-l} - \tilde{x}^{(m)} e^{j\theta} \right|^2} p_{lm} \right] && (2.8)
\end{aligned}$$

where $\tilde{x}^{(m)}$ is the m-th QAM symbol belonging to the constellation $\mathscr{X}$ and

$$p_{lm} \triangleq P(x_{k-l} = \tilde{x}^{(m)}|\boldsymbol{r}).$$

In other words, p_{lm} is the probability that the symbol transmitted at time $k-l$ is equal to the m-th symbol of the QAM constellation.

Note that in (2.6) and (2.7) the order of summation and product operators are exchanged and: this is justified in Appendix A.

One can now take the natural logarithm, thus obtaining

$$\begin{aligned}
\hat{\theta}_k &\simeq \underset{\theta}{\operatorname{argmax}} \ln \prod_{l=0}^{\ell-1} \left[\sum_{m=0}^{M-1} \frac{1}{2\pi\sigma^2} e^{-\frac{1}{2\sigma^2}\left| r_{k-l} - \tilde{x}^{(m)} e^{j\theta} \right|^2} p_{lm} \right]\\
&= \underset{\theta}{\operatorname{argmax}} \sum_{l=0}^{\ell-1} \ln \left[\sum_{m=0}^{M-1} \frac{1}{2\pi\sigma^2} e^{-\frac{1}{2\sigma^2}\left| r_{k-l} - \tilde{x}^{(m)} e^{j\theta} \right|^2} p_{lm} \right].
\end{aligned}$$

A key assumption now is to operate in the low SNR regime, which is a typical condition for powerful error correcting codes. In this case, the following approximations can be used:

$$\begin{aligned}
e^x &\simeq 1 + x \qquad |x| \ll 1 && (2.9)\\
\ln(1+y) &\simeq y \qquad |y| \ll 1. && (2.10)
\end{aligned}$$

It is therefore possible to write

$$\begin{aligned}
\hat{\theta}_k &\simeq \underset{\theta}{\operatorname{argmax}} \sum_{l=0}^{\ell-1} \ln \left[\frac{1}{2\pi\sigma^2} \sum_{m=0}^{M-1} p_{lm} \left\{ 1 + \frac{\left| r_{k-l} - \tilde{x}^{(m)} e^{j\theta} \right|^2}{2\sigma^2} \right\} \right] \\
&= \underset{\theta}{\operatorname{argmax}} \sum_{l=0}^{\ell-1} \ln \left[\frac{1}{2\pi\sigma^2} \left\{ 1 + \sum_{m=0}^{M-1} p_{lm} \frac{\left| r_{k-l} - \tilde{x}^{(m)} e^{j\theta} \right|^2}{2\sigma^2} \right\} \right] \\
&= \underset{\theta}{\operatorname{argmax}} \sum_{l=0}^{\ell-1} \ln \frac{1}{2\pi\sigma^2} + \sum_{l=0}^{\ell-1} \ln \left[1 + \sum_{m=0}^{M-1} p_{lm} \frac{\left| r_{k-l} - \tilde{x}^{(m)} e^{j\theta} \right|^2}{2\sigma^2} \right] \\
&= \underset{\theta}{\operatorname{argmax}} \sum_{l=0}^{\ell-1} \ln \left[1 + \sum_{m=0}^{M-1} p_{lm} \frac{\left| r_{k-l} - \tilde{x}^{(m)} e^{j\theta} \right|^2}{2\sigma^2} \right].
\end{aligned}$$

where the first low SNR regime approximation (2.9) has been used and irrelevant terms have been dropped. Using the second low SNR regime approximation (2.10) and dropping irrelevant terms leads to

$$\begin{aligned}
\hat{\theta}_k &\simeq \underset{\theta}{\operatorname{argmax}} \sum_{l=0}^{\ell-1} \sum_{m=0}^{M-1} p_{lm} \frac{\left| r_{k-l} - \tilde{x}^{(m)} e^{j\theta} \right|^2}{2\sigma^2} \\
&= \underset{\theta}{\operatorname{argmax}} \sum_{l=0}^{\ell-1} \sum_{m=0}^{M-1} p_{lm} \left\{ |r_{k-l}|^2 + |\tilde{x}^{(m)}|^2 + 2\Re \left[r_{k-l} \left(\tilde{x}^{(m)} \right)^* e^{-j\theta} \right] \right\} \\
&= \underset{\theta}{\operatorname{argmax}} \sum_{l=0}^{\ell-1} |r_{k-l}|^2 \underbrace{\sum_{m=0}^{M-1} p_{lm}}_{=1} + \sum_{l=0}^{\ell-1} \sum_{m=0}^{M-1} p_{lm} |\tilde{x}^{(m)}|^2 + \sum_{l=0}^{\ell-1} \sum_{m=0}^{M-1} p_{lm} 2\Re \left[r_{k-l} \left(\tilde{x}^{(m)} \right)^* e^{-j\theta} \right] \\
&= \underset{\theta}{\operatorname{argmax}} \sum_{l=0}^{\ell-1} \sum_{m=0}^{M-1} p_{lm} \Re \left[r_{k-l} \left(\tilde{x}^{(m)} \right)^* e^{-j\theta} \right].
\end{aligned}$$

Therefore, after further (simple) manipulations one obtains:

$$\hat{\theta}_k \simeq \underset{\theta}{\operatorname{argmax}} \Re \left[\sum_{l=0}^{\ell-1} r_{k-l} \alpha_{k-l}^* e^{-j\theta} \right] \tag{2.11}$$

where

$$\alpha_{k-l} \triangleq \sum_{m=0}^{M-1} p_{lm} \tilde{x}^{(m)}$$

represents the center of gravity of the QAM constellation, at time instant $k-l$, based on the symbol APPs.

Denote as $\hat{\theta}^{(i)}$ the phase estimate over the i-th ℓ-symbol block, i.e.,

$$\hat{\theta}_k = \hat{\theta}^{(i)} \qquad k = (i-1)\ell+1,\ldots,i\ell \qquad i = 1,2,\ldots,n_{\mathrm{p}}$$

where n_{p} is the number of disjoint blocks with length ℓ within the same codeword.[1] Denoting the ℓ observables in the i-th block as $\boldsymbol{r}^{(i)} \triangleq [r_{(i-1)\ell+1},\ldots,r_{i,\ell}]$, under the assumption of constant phase over this block, its phase estimate for the k-th symbol in the i-th block, $k=(i-1)\ell+1,\ldots,i\ell$, can be obtained from (2.11) and expressed as

$$\hat{\theta}_{k,\mathrm{BW}} = \arg\left[\sum_{l=0}^{\ell-1} r_{i\ell-l}\alpha_{i\ell-l}^{*}\right] = \arg\left[\Phi_{i\ell,\ell}^{\mathrm{APP}}\right] \tag{2.12}$$

where the subscript BW has been introduced to clearly indicate the BW strategy and

$$\begin{aligned} \Phi_{j,\ell}^{\mathrm{APP}} &\triangleq \sum_{l=0}^{\ell-1} r_{j-l}\alpha_{j-l}^{*} \\ \alpha_{i\ell-l} &\triangleq \sum_{m=0}^{M-1} p_{lm}\tilde{x}(m) \\ p_{lm} &\triangleq P(x_{i\ell-l}=\tilde{x}(m)|\boldsymbol{r}). \end{aligned} \tag{2.13}$$

The quantity $\alpha_{i\ell-l}$ can be interpreted as the *center of gravity*, at epoch $i\ell-l$, of the transmitted constellation under the assumption that each constellation symbol is weighted by the corresponding APP. If a given symbol $\tilde{x}(m)\in\mathscr{X}$ has probability close to 1 at epoch $i\ell-l$, then $\alpha_{i\ell-l}\simeq\tilde{x}(m)$; on the other hand, if no APP is available (this happens at the initial "coarse" phase estimation), then $\alpha_{i\ell-l}$ corresponds to the unweighted center of the constellation. If $x_{i\ell-l}$ is a pilot symbol, then $\hat{\alpha}_{i\ell-l}=x_{i\ell-l}$.

The quantities $\{p_{lm}\}$ are the APPs, derived from the soft-output information generated by the decoder, that the symbol transmitted at epoch $i\ell-l$ is equal to the m-th symbol, belonging to constellation set $\mathscr{X}$ and denoted as $\tilde{x}(m)$. Note that their computation is independent of the presence/absence of multi-level coding. If multi-level

[1] The subscript k denotes the symbol index and the superscript i the i-th block.

coding is not considered, all bit LLRs (used to compute a symbol APP) can be obtained by the channel decoder; otherwise, $b - b_1$ free bit LLRs come directly from the (soft-output) demapper. Since an M-ary symbol x_k is labeled by $b = \log_2 M$ bits $(c_k^{(1)}, \ldots, c_k^{(b)})$, one obtains

$$P(x_{i\ell-l}|\boldsymbol{r}) = \prod_{j=1}^{\log_2 M} P(c_{i\ell-l}^{(j)}|\boldsymbol{r}) = \prod_{j=1}^{\log_2 M} \frac{e^{\left(1-c_{i\ell-l}^{(j)}\right)\mathscr{L}_{i\ell-l}^{(j)}}}{1+e^{\mathscr{L}_{i\ell-l}^{(j)}}}$$

where

$$\mathscr{L}_{i\ell-l}^{(j)} \triangleq \ln \frac{P(c_{i\ell-l}^{(j)}=0|\boldsymbol{r})}{P(c_{i\ell-l}^{(j)}=1|\boldsymbol{r})} \qquad j = 1, \ldots, \log_2 M$$

are the LLRs output either by the soft-output channel decoder (coded bits) or by the soft-output demapper (free bits).

2.2.2 Sliding Window

Different alternative schemes for phase noise estimation are possible, as shown in Figure 2.3, in order to smooth and track the correct phase value.

Sliding Window (SW)-based phase noise estimation approach extends the BW approach, to enhance the performance of the phase estimation algorithm by relying on an improved use of (2.12). The BW phase estimation algorithm considers disjoint sets of observables in the the phase noise estimation, i.e., the estimated phase for a length-ℓ window is used to derotate the symbols over the same block and is, in general, different from those estimated in adjacent blocks, as shown in Figure 2.3 (a). However, there exists a step-wise trend in adjacent blocks of estimated phases.

In SW approach, the block estimated phase are associated to the observable in the middle of the window for each sliding position, as shown in Figure 2.3 (b). Mathematically,

$$\hat{\theta}_{k,\mathrm{SW}} = \arg\left[\Phi_{k\ell-\lfloor \ell/2 \rfloor,\ell}^{\mathrm{APP}}\right] \tag{2.14}$$

It can be observed that

$$\Phi_{k\ell-\lfloor \ell/2 \rfloor,\ell}^{\mathrm{APP}} = \sum_{j=0}^{\ell-1} r_{k\ell-j}\alpha_{k\ell-j}^{*} \tag{2.15}$$

From a practical implementation viewpoint, one should observe that border effects arise at the beginning and the end of the frame in (2.15). In fact, the phase estimate derived from the ℓ-observable block is associated with the symbol at position $\lfloor \ell/2 \rfloor$. These border effects are managed through secondary windows of smaller sizes ($\ell_2 < \ell$) at the beginning and at the end of the frame. Finally, note also that the complexity of the SW approach is higher than that of the BW approach in terms of time and computational load, since the block-based phase estimation needs to be performed for each observable r_k.

2.2.3 Phasor Linear Prediction

The BW strategy is based on the use of disjoint consecutive ℓ-symbol windows. An interesting extension leads to the use of an ℓ-symbol sliding window. In particular, for the generic k-th symbol assume $k \geq \ell$ to avoid border effects. There are ℓ consecutive ℓ-symbol blocks including the k-th symbol. In particular, taking into account the definition (2.12), the following phase estimate at epoch k can be considered:

$$\hat{\theta}_{k,\mathrm{PLP}} = \arg \left[\sum_{i=0}^{\ell-1} \Phi_{k+i,\ell}^{\mathrm{APP}} \right] \tag{2.16}$$

where the subscript PLP denotes the Phasor Linear Prediction. It can be observed that

$$\sum_{i=0}^{\ell-1} \Phi_{k+i,\ell}^{\mathrm{APP}} = \sum_{j=-\ell+1}^{\ell-1} u_j r_{k-j} \alpha_{k-j}^{*} \tag{2.17}$$

where $u_j \triangleq \ell - |j|$, $j \in \{-\ell+1, \ldots, \ell-1\}$. Therefore, (2.16) can be written as follows:

$$\hat{\theta}_{k,\mathrm{PLP}} = \arg \left[\sum_{j=-\ell+1}^{\ell-1} u_j r_{k-j} \alpha_{k-j}^{*} \right] \tag{2.18}$$

The phase estimation strategy (2.18) is a generalized (APP-based) instance of the PLP approach to phase estimation proposed in [45]. In particular, in (2.17) and (2.18) the weighting coefficients $\{u_j\}$ have a triangular shape and provide the highest weight to the k-th observable and is referred here to as APP-based PLP.

2.2.4 Use of Filtering Approaches

To further enhance the system performance, additional approaches can be obtained by properly filtering the estimation metric to smooth the phase estimation as suggested in [46]. Accordingly, (2.12) can be modified as

$$\hat{\theta}_k = \arg\left[\sum_{l=-\ell/2}^{\ell/2} p_l r_{k\ell-l}\alpha_{k\ell-l}^*\right] \tag{2.19}$$

where the filter weights $\{p_l\}$ can be set according to a bi-exponential shape [46], i.e.,

$$p_l = \xi^{|l|}$$

where ξ, $0 \leq \xi \leq 1$, is a suitable parameter to be optimized by trial and error for the phase noise dynamics of interest. The corresponding algorithms will be denoted as Weighted SW (WSW) and Weighted PLP (WPLP), respectively.

2.3 Iterative Receiver Structure

We now describe the iterative receiver, shown as the right-most block in Figure 2.1, which relies on the APP-based phase estimation algorithms derived in Section 2.2. The detailed scheme of the iterative synchronization and decoding receiver is shown in Figure 2.4, in which element-wise vector products are present. The dashed line is only needed for multi-level coding.

The phase noise of the received observables $\{r_k\}$ in (2.3) is pre-compensated by means of an interpolator which estimates the phase process on the basis of pilot symbols. In this work, we only consider a simple linear interpolator, which limits the system delay [47], with $N_\mathrm{p} = 1$. In correspondence to pilot symbols, the phase noise process is simply estimated as the difference between the phase of the received sample and the phase of the transmitted symbol x_k:

$$\hat{\theta}_k = \angle r_k x_k *.$$

Note that this estimation is asymptotically (at high SNR) exact. Then, the phase noise which impacts the data symbols is pre-estimated by means of linear interpolation be-

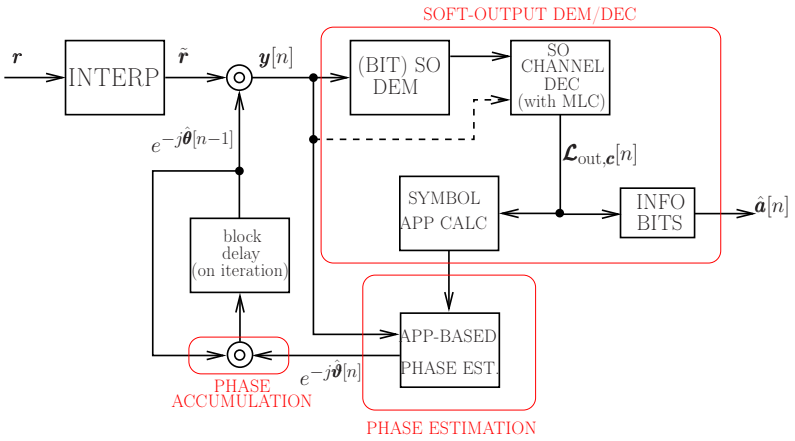

Figure 2.4: Iterative synchronization and decoding receiver for the APP-based separate phase estimation algorithms, where dashed line refers to the instances with multi-level coding.

tween the phases of two consecutive pilot symbols. This preliminary phase estimation enables to carry out the first decoding iteration, which is necessary to perform an APP-based phase estimation. The observable at the output of the interpolator, denoted as $\tilde{r}_k$, can be expressed as follows:

$$\tilde{r}_k = r_k e^{-\hat{\theta}_{k,\text{int}}} = x_k e^{\left(\theta_k - \hat{\theta}_{k,\text{int}}\right)} + n'_k$$

where $e^{-\hat{\theta}_{k,\text{int}}}$ is the derotation introduced by the pre-compensation block. The additive noise process $\{n'_k\}$ is still i.i.d. Gaussian. The new phase noise process $\{\theta_k - \hat{\theta}_{k,\text{int}}\}$ can no longer be characterized by the same model of $\{\theta_k\}$, e.g., a Wiener model. However, the APP-based synchronization algorithms proposed in Section 2.2 do not require any a priori statistical characterization of the phase noise and, therefore, can be applied directly.

After the initial interpolation, the observables $\{\tilde{r}_k\}$ are fed directly to the input of the demodulator, whose soft outputs are then passed to the soft-input soft-output decoder, which possibly takes into account the multi-level coding scheme. The soft-output decoder generates LLRs on the (multi-level) coded bits, denoted as $\mathcal{L}_{\text{out},c}[n]$,

where n refers to the iteration number and the vector collects the values for all symbols in a codeword. This first demodulation/decoding step is referred to as 0-th iteration (i.e., $n = 0$).

In the absence of multi-level coding, the decoder is a standard channel decoder (e.g., message passing for LDPC codes). In the presence of multi-level coding, instead, multi-stage decoding [37] is performed: the soft-output information associated with the coded bits is given by the channel decoder, whereas that associated with the free bits is computed according to the (multi-level coding) scheme in Section 2.1.1. Specifically, from the soft output information on the channel coded bits, one can compute the most likely code binary sequence. For $b_1 = 4$ and $b > b_1$, each 4 decided code bits identify a subset associated with a sub-constellation of size 2^{b-4}, corresponding to $b-4$ free bits. At this point, one can compute the soft output on the free bits based on this sub-constellation. The LLRs on the channel coded bits and on the free bits can then be combined to generate APPs on the constellation symbols. The APPs then feed the phase estimator. We refer to a sequence of phase estimation and demodulation/decoding as an iteration. In the presence of channel coding with iterative decoding, e.g., LDPC or turbo coding, we can refer to the iterations between the phase estimation block and the demodulation/decoding block as "external" iterations, in order to distinguish them from "internal" iterations of the decoder.

The iterative algorithm can now be summarized as follows. We denote as n_{it} the maximum number of (external) iterations between phase estimator and demapper/decoder. The 0-th iteration, i.e., the first demodulation/decoding act that follows interpolation has been described above. At the n-th iteration ($n = 1, \ldots, n_{\text{it}}$), the phase estimator operates on the observable vector $\boldsymbol{y}[n]$ obtained as

$$\boldsymbol{y}[n] = \tilde{\boldsymbol{r}} \circ e^{-\hat{\boldsymbol{\theta}}[n-1]} \tag{2.20}$$

where the vectors $\boldsymbol{y}[n]$, $\tilde{\boldsymbol{r}}$, and $\hat{\boldsymbol{\theta}}[n-1]$ can be defined by analogy with vector $\boldsymbol{r}$, $\boldsymbol{\theta}[0] = \boldsymbol{0}$, and the symbol $\circ$ represents the Hadamard (or element-wise) product between two vectors. Note that the exponential function is applied element-wise to the vector $\hat{\boldsymbol{\theta}}[n-1]$. The observable $\boldsymbol{y}[n]$ is then fed to the demapping and decoding functions to compute the APPs on transmitted symbols to be used in (2.12), (2.14),(2.18), or (2.19)

for their respective phase noise estimation algorithms, accordingly. Note that, since the derotated observable $\boldsymbol{y}[n]$ is used, the estimated phase corresponds to a residual phase error $\hat{\boldsymbol{\theta}}[n]$, which is accumulated to obtain the phase estimate

$$\hat{\boldsymbol{\theta}}[n] = \hat{\boldsymbol{\theta}}[n-1] + \hat{\boldsymbol{\theta}}[n]. \tag{2.21}$$

to be used in (2.20). After n_{it} iterations, a final decision on the vector of transmitted bits in a codeword, denoted as $\hat{\boldsymbol{a}}$, is emitted.

2.4 Performance Analysis

In this section, we present a performance analysis of the proposed phase estimation algorithm and its extensions. In Sub-section 2.4.1, we show numerical results in terms of Bit Error Rate (BER) and Mean Square Error (MSE). In particular, the MSE is defined as

$$\text{MSE} \triangleq \frac{1}{n}\sum_{i=1}^{n}(\hat{\theta}_i - \theta_i)^2 \tag{2.22}$$

being n the number of considered symbols. The $\hat{\theta}_i$ is a block-constant, i.e.,

$$\hat{\theta}_i = \hat{\theta}_k \qquad i = (k-1)\ell + 1, \ldots, k\ell$$

for a given block index k. In Sub-section 2.4.2, we extend the performance analysis to compare the complexity of the proposed algorithms with joint-MAP based solution for phase noise estimation proposed in [48].

2.4.1 Numerical Results

In this section, we investigate the performance, in terms of BER, of the proposed receiver schemes with iterative synchronization and demodulation/decoding for a coded high-order QAM scheme. $N_{\text{p}} = 1$ pilot symbol is inserted in the frame every $N = 48$ symbols and belongs to a 4-QAM constellation with average energy 2.5 times the average energy of data symbols—this corresponds to an energy penalty $1 + q = 0.212$ dB. The channel code is an LDPC code with rate $R = k/n = 7/8$,

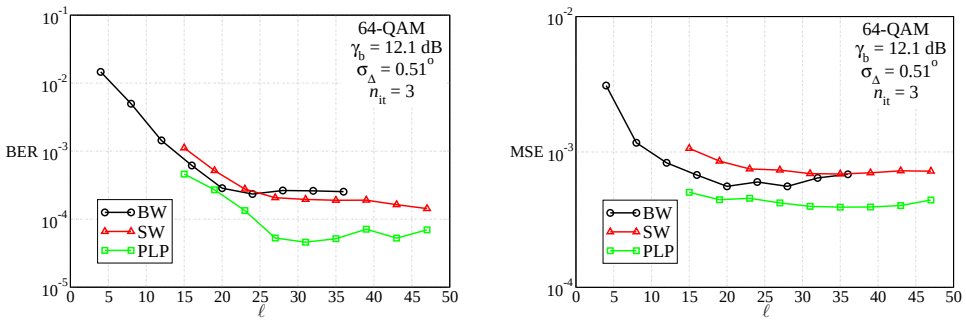

(a) (b)

Figure 2.5: Performance, as functions of ℓ, for BW, SW, and PLP approaches, considering 64-QAM, $\sigma_\Delta = 0.51°$, $\gamma_b = 12.1$ dB, and $n_{it} = 3$: (a) BER and (b) MSE.

with $k = 7056$ and $n = 8064$. The exponent parity-check matrix construction (semi-random technique) and the encoding algorithm of the used LDPC code are those of the WiMAX standard [49, Paragraph 8.4.9.2.5, Annex H]. In particular, the exponent parity-check matrix has $n_{b,r} = 12$ rows, $n_{b,c} = 96$ columns, a spreading factor $Z_f = 84$, a constant row weight $w_r = 32$ and an average column weight $w_c = 4$. LDPC decoding is based here on the sum-product algorithm, where at the end of each internal iteration the algorithm verifies the parity check equation of the code and stops if it is satisfied. The maximum number of internal iterations is set to 50—our results show that for BER values below 10^{-2} the number of required internal iterations is lower than 5.

In Figure 2.5, we show (a) the BER and (b) the MSE, as functions of ℓ, for the BW, SW, and PLP approaches, considering 64-QAM, $\sigma_\Delta = 0.51°$, $\gamma_b = 12.1$ dB, and $n_{it} = 3$. From Figure 2.5 (a), one can observe that the BW approach has a minimum BER for $\ell = 24$, whereas the SW approach performs best for $\ell \geq 27$. It can also be observed that PLP phase estimation algorithm performs significantly better than BW and SW algorithms for $\ell \geq 23$ and the optimized window length for PLP approach is $\ell = 31$. Similar considerations can be carried out from the MSE performance results in Figure 2.5 (b).

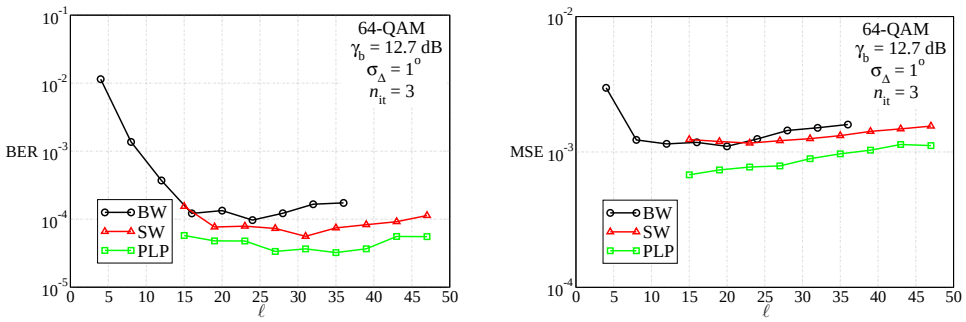

Figure 2.6: Performance, as functions of ℓ, for BW, SW, and PLP approaches, considering 64-QAM, $\sigma_\Delta = 1^\circ$, $\gamma_b = 12.7$ dB, and $n_{it} = 3$: (a) BER and (b) MSE.

In Figure 2.6, we show (a) the BER and (b) the MSE, as functions of ℓ, for the BW, SW, and PLP approaches, considering 64-QAM, $\sigma_\Delta = 1^\circ$, $\gamma_b = 12.7$ dB, and $n_{it} = 3$. According to BER results in Figure 2.6 (a), the optimal values of the window length ℓ are: 24 for BW; 31 for SW; and 39 for PLP. Similar considerations can be carried out from the MSE results in Figure 2.6 (b).

Figure 2.7 presents simulation results about the impact of the biexponentially-shaped filtering technique presented in Section 2.2.4. This technique is applied to both SW and PLP and the MSE is shown, as a function of ξ, for 64-QAM, $\gamma_b = 11.9$, $\sigma_\Delta = 0.51^\circ$, and $n_{it} = 3$ iterations.

When WSW is considered, there is a slight improvement for large values of the filtering parameter, e.g., $\xi = 0.9$. On the other hand, when WPLP is considered no such improvement arises. This is due to the fact that SW and PLP are already modified versions of the BW strategy and, therefore, the phase estimate is already smooth.

At this point, we compare the proposed strategies in Figure 2.8. The BER is shown, as a function of bit SNR, for 64-QAM, $\sigma_\Delta = 0.51^\circ$, comparing BW, SW, and PLP for various of the window length and of the number of iterations. It can be observed that PLP outperforms the other approaches (BW and SW). Moreover, SW has approximately the same performance of the BW approach. Note that similar

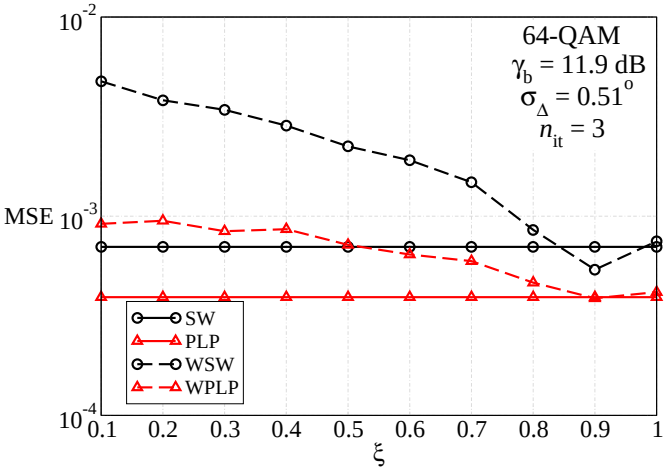

Figure 2.7: Impact of filtering on SW and PLP: MSE, as a function of ξ, for 64-QAM, $\gamma_b = 11.9$, $\sigma_\Delta = 0.51°$, and 3 iterations.

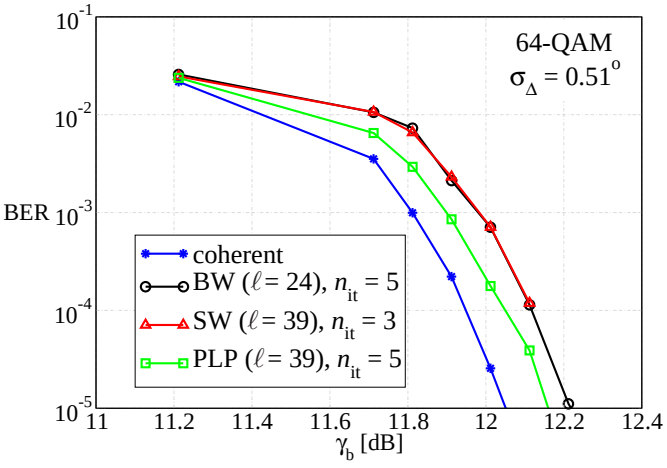

Figure 2.8: BER, as a function of bit SNR, for 64-QAM, $\sigma_\Delta = 0.51°$, comparing BW, SW, and PLP under different window lengths and number of iterations.

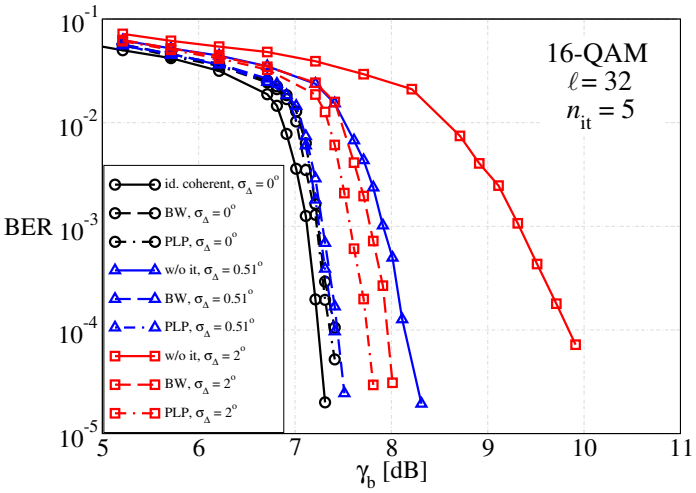

Figure 2.9: BER, as a function of bit SNR, for 16-QAM. Different phase noise intensities are considered as shown in the legends for equal number of iterations.

results hold for other values of the phase noise intensity.

In Figure 2.9, the BER is shown, as a function of bit SNR, for BW and PLP, $n_{\text{it}} = 5$, phase noise intensities, and 16-QAM is considered. For $\sigma_\Delta \leq 2^\circ$ the loss with respect to the reference coherent system (i.e., the performance of the considered system with $\sigma_\Delta = 0^\circ$) is 0.2 dB. On the other hand, there is a loss of 0.5 dB for $\sigma_\Delta = 2^\circ$. It can be noticed that the PLP approach performs better than the BW-based phase estimation algorithm at the cost of slightly higher computational complexity.

In Figure 2.10, 1024-QAM is considered and the loss is approximately 0.2 dB for $\sigma_\Delta = 0.2^\circ$, while the system performance degrades by 0.5 dB when $\sigma_\Delta = 0.25^\circ$. Note that, as suggested in Figure 2.5 and Figure 2.6 for 64-QAM, proper window length optimization can be performed to enhance the performance of the system for a particular modulation order.

From Figure 2.5 and Figure 2.6, one can conclude that $\ell = 32$ to be a good compromise value for constellation sizes from 16- to 1024-QAM and several phase noise intensities, for both BW and PLP. In Figure 2.11, the BER is shown, as a function of γ_b, for 1024-QAM, $\sigma_\Delta = 0.21^\circ$, 5 iterations, and window length $\ell = 32$—similar

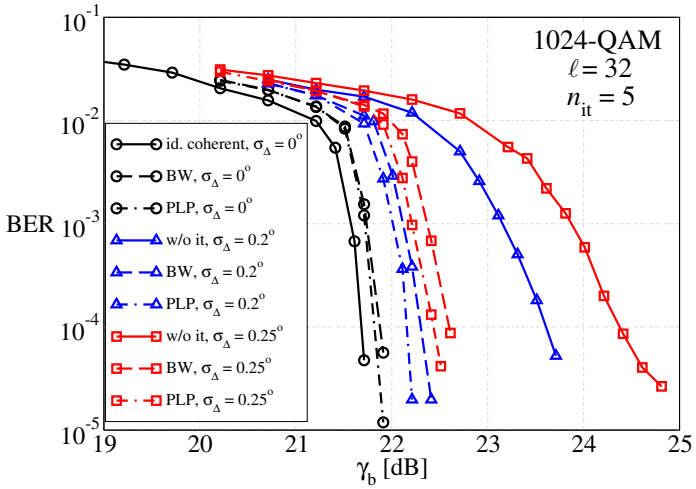

Figure 2.10: BER, as a function of bit SNR, for 1024-QAM. Different phase noise intensities are considered as shown in the legends for equal number of iterations.

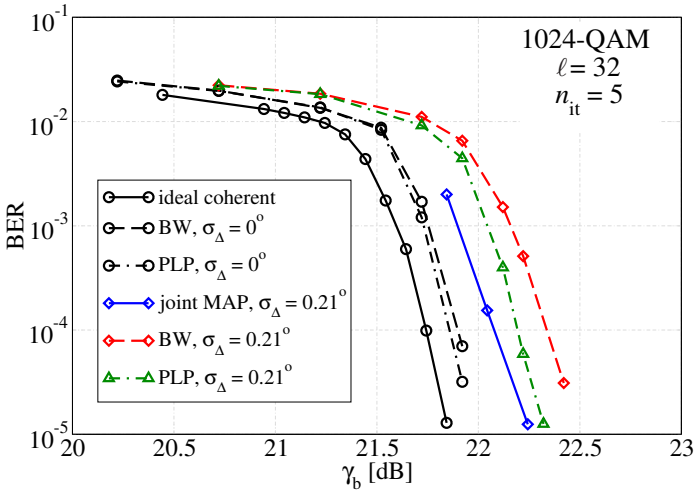

Figure 2.11: BER, as a function of γ_b, for 1024-QAM, $\sigma_\Delta = 0.21°$, $n_{it} = 5$ iterations, and $\ell = 32$. The proposed algorithms (BW and PLP) are compared with that joint MAP for equal number of iterations.

results hold for other parameter settings. The performance of the proposed iterative schemes (with BW and PLP phase estimation strategies) is compared with the performance of the joint iterative decoding and synchronization receiver proposed in [48] operating on $\boldsymbol{r}$, in which pilot symbols are exploited to derive APPs on data symbols (denoted as "joint MAP"). One can easily observe that the joint MAP scheme slightly outperforms the proposed schemes: in particular, the PLP scheme shows a 0.1 dB loss with respect to the joint MAP scheme. The higher-order modulation are sensitive to phase noise, and the 0.1 dB loss for higher modulation for PLP based separate approach is negligible.

Unlike our solution, the joint MAP approach of [48] requires an iterative receiver working on a properly designed factor graph (rather than using off-the-shelf demodulation and decoding blocks and a separate synchronizer) and knowledge of the phase noise intensity. In fact, the algorithm in [48], although designed for a Wiener phase noise model, exhibits a good behaviour also for more realistic phase noise statistics, provided that the value of σ_Δ is optimized in order to maximize the performance.

2.4.2 Complexity Issues

The computational complexity can be evaluated in terms of the number of real multiplications and additions, per modulation symbol and external iteration, required for phase synchronization and generation of LLRs at the input of the soft-input soft-output decoder. Assuming that one complex multiplication requires four real multiplications and two real additions, our analysis shows that the number of multiplications is $8+18M$ for joint MAP and asymptotically $5M$ (large M) for BW and PLP, whereas the number of additions is $8+M(11+\log_2 M)$ for joint MAP[2] and asymptotically $5M$ for BW and PLP [51]. On the basis of these results, one can define the computational gains achieved by the proposed algorithms as the ratio between the number of multiplications (additions) required by joint MAP and the number of multiplications (additions) required by the proposed solutions. These computational

[2]The complexity evaluations for the joint MAP algorithm, here derived independently, comply with those reported in [50, Table I].

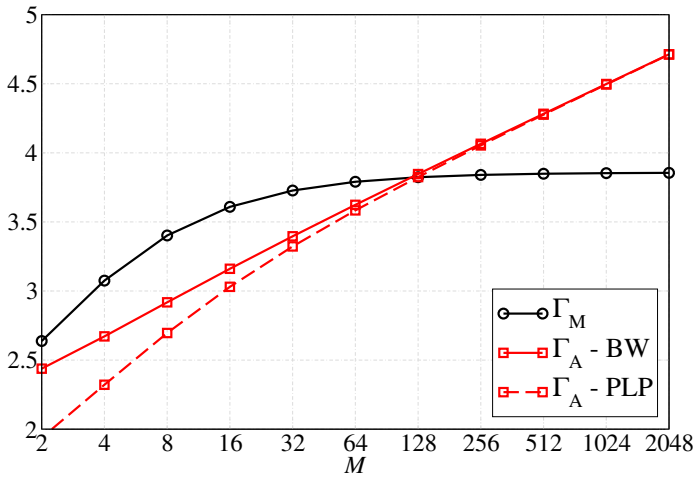

Figure 2.12: Computational gains, as functions of M, of the proposed synchronization algorithms, with respect to joint MAP, for the considered simulation settings.

gains, denoted as Γ_{M} for multiplications and Γ_{A} for additions, are shown, as functions of M, in Figure 2.12.

The overall computational gains of our approach, with respect to [48], increase with the constellation size. More specifically, both BW and PLP approaches are significantly less computationally complex for medium-high QAM constellation orders.

2.5 Concluding Remarks

In this chapter, a novel low-complexity pilot symbol-aided iterative synchronization and decoding scheme with separate MAP phase estimation is proposed. The proposed approach, in particular the PLP phase estimation strategy, guarantees a good performance for both small and medium-high constellation sizes, even for challenging phase noise scenarios and complete absence of statistical information about the phase noise process. At the cost of a minor performance degradation with respect to optimized joint synchronization/decoding approaches, the proposed solution exhibits

a significantly lower computational complexity and its pragmatic structure is tailored to exploit off-the-shelf subsystems, thereby representing an attractive solution from a practical implementation viewpoint.

Chapter 3

Phase Synchronization for Channel impaired by ISI

In this chapter, we propose an iterative synchronization and decoding algorithm with improved robustness of the phase noise impaired communication system. In particular, we assume oversampling (more that one sample per symbol interval) at the receiver. A low-complexity Maximum A-posterior Probability (MAP) iterative synchronization algorithm is derived to perform sliding window-based phase estimation.

The rest of the chapter is structured as follows. In Section 3.2, the system model for the considered system is presented. In Section 3.3, the proposed APP-based synchronization algorithm. The corresponding iterative synchronization receiver structure is shown in Section 3.4 and performance analysis is carried out in Section 3.5. Finally, Section 3.6 concludes the chapter.

3.1 Introduction

Phase noise causes distortion or complete loss of incoming information in traditional receivers and, consequently, high Bit Error Rate (BER). The performance of communication systems over phase noise channels has been investigated from different perspectives. A very common assumption consists in assuming slowly varying phase

noise over a symbol duration [51, 52], which will be here referred to as "symbol-time" model. In this case, both channel and receiver can be exactly characterized by only one sample per symbol-time [9]. The Information Rate (IR) of a symbol-time phase noise channel is studied in [11, 12]. The IR with a multi-sample receiver, i.e., which employs more than one sample per symbol, has been investigated in [12, 53], showing promising theoretical gains.

Many methods for estimating the phase noise introduced by an unknown channel have been proposed over the past few decades, from a simple Phase Locked Loop (PLL) to sophisticated iterative detection/decoding schemes to achieve better phase noise tolerance with lower computational complexity [48, 51, 52]. Theoretical analysis of an oversampled tracking of phase noise is performed in [54], whereas joint symbol detection and tracking in the multi-receiver has shown robust performance [55–57].

The use of oversampling leads to the presence of memory because of Inter-Symbol Interference (ISI), which is a well studied transmission impairment. To calculate the exact APPs at symbol time, one can use reduced-complexity BCJR algorithms as suggested in [58–60]. However, BCJR algorithms are practical as long as an ISI channel has a trellis with a sufficiently small number of states and small constellation sizes. Additionally, they also require the statistical information of the noise process. In contrast to BCJR equalization, block-wise processing with soft ISI cancellation and detection can be regarded as a pragmatic solution for medium to higher-order modulations [61].

In this work, we extend the work presented in [51] to a multi-sample receiver for the phase noise channel, managing the generated ISI in the received sequence. The purpose of this work is to exploit the received information from the channel by exchanging the information in an iterative fashion to achieve robust convergence [62].

We consider the well-known shaping pulse with Square Root Raised Cosine (SRRC) Fourier transform with a linear quadrature amplitude modulation (QAM). An efficient Maximum A posteriori Probability (MAP)-based iterative synchronization algorithm is devised. The phase estimation algorithm exploits the A Posteriori Probabilities (APPs) of the transmitted samples and a sliding window-based phase

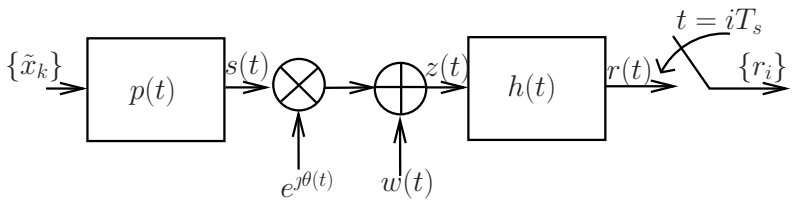

Figure 3.1: System model for the continuous-time phase noise channel.

estimation algorithm to perform phase estimation on each received sample. Our results with Low-Density Parity-Check (LPDC)-coded 64-QAM scheme show good performance with respect to an equivalent traditional receiver which uses only one sample per symbol time.

3.2 System Model

3.2.1 Continuous-time Channel Model

The considered phase noise channel is shown in the Figure 3.1. The received signal $z(t)$ is given by

$$z(t) = s(t)e^{j\theta(t)} + w(t) \tag{3.1}$$

where $s(t) = \sum_{k=-\infty}^{\infty} \tilde{x}_k p(t-kT)$ is the transmitted signal with $\{\tilde{x}_k\}$ being the information sequence and $p(t)$ is a unit-energy pulse shape. The communication channel introduces AWGN $w(t)$ and phase noise $e^{j\theta(t)}$. The phase noise is modeled as a Wiener process generated by integrating a white Gaussian process and characterized by zero-mean Power Spectral Density (PSD) $2\pi B_\theta$. Note that the phasor $e^{j\theta(t)}$ has a Lorentzian PSD and exhibits 3-dB spectral width B_θ.

As pulse shaping, we consider SRRC pulse shape, which can be expressed as

$$p(t) = 4\beta \frac{\cos[(1+\beta)\pi\frac{t}{T}] + \frac{\sin[(1-\beta)\pi\frac{t}{T}]}{4\beta\frac{t}{T}}}{\pi\sqrt{T}[1-(4\beta\frac{t}{T})^2]}$$

where the sample interval is $T_s = 1/f_s$ (dimension: [s]) and β is the roll-off factor,

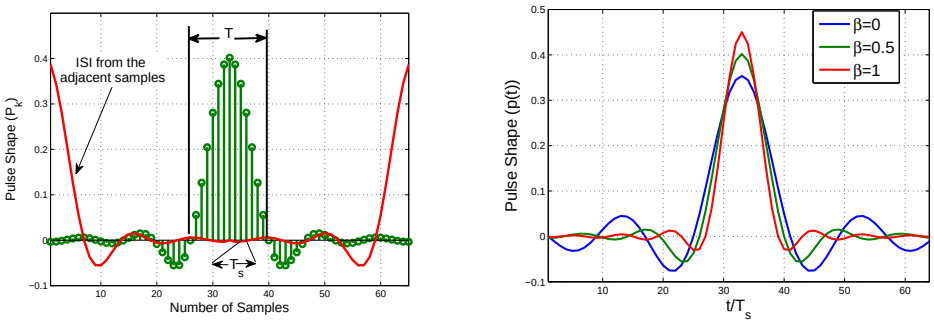

(a) (b)

Figure 3.2: Characteristics of SRRC pulse shapes (a). Symbol time $\{T\}$ and sampling time $\{T_s\}$ comparison for SRRC pulse shape at $\beta = 0.5$, $N_u = 8$, $L = 65$, (b). SRRC pulse shapes for different β, as time function t.

with $0 \leq \beta \leq 1$. Some characteristics of the SRRC pulse shape are shown in Figure 3.2. It can be noticed that the ISI reduces with an increase in the β, however $\beta = 0.3 - 0.7$ are commonly used roll-offs in wireless communication system. The SRRC pulse shapes satisfy the Nyquist criterion, leading to no ISI at symbol-time. The signal bandwidth for the bandlimited pulse with SRRC transform is strictly limited to $B = (1+\beta)/2T$.

At the receiver side, we consider a front-end filter $h(t)$, which is given by the convolution of the transmitter pulse with the channel response, having bandwidth B_h and frequency response $H(f)$, such that

$$|H(f)|^2 = \begin{cases} 1 & |f| \leq B \\ \text{arbitrary} & B < |f| < B_h \\ 0 & \text{otherwise.} \end{cases} \tag{3.2}$$

It follows that the useful signal is not attenuated by the filtering operation, since the frequency response is unitary in the signal bandwidth.

In the absence of phase noise, if sampling with period $T_s < 1/2B_h$ is performed, the sampled sequence $\{r_i\}$ is a sufficient statistic for the detection of the transmitted

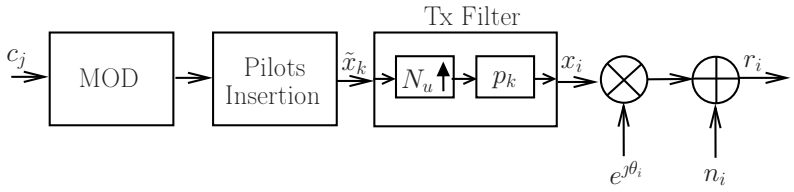

Figure 3.3: An equivalent discrete-time system model.

sequence [63]. Moreover, taking into account $|H(f)|^2$ has vestigial symmetry with respect to $1/2T_s$, sampling at multiple of time instant T_s leads to independent and identically distributed (i.i.d.) thermal noise samples. In order to simplify the front-end implementation, one can assume T_s as an integer fraction of T, i.e., $T_s = T/N_u$, where N_u is the oversampling factor. A practical receiver front-end able to deal with signal bandwidth B can use a filter as in (3.2) with vestigial symmetry at $N_u/(2T)$ and bandwidth

$$\frac{N_u}{2T} < B_h < \frac{N_u}{T} - B.$$

The output signal sampled at rate N_u/T to provide a sufficient statistic with i.i.d. noise samples.

3.2.2 Discrete-time Channel Model

An equivalent discrete-time system model is shown in Figure 3.3. At the transmitter, the information symbols $\{\tilde{x}_k\}$ are generated in the following way. A binary information sequence $\{a_i\}$ is encoded into a sequence $\{c_j\}$ through a binary channel code with rate R. A modulation scheme with constellation size $M = 2^b$ and symbol energy E_s is then used. In particular, we consider M-QAM constellations with multi-level coding (MLC) [37], such that b_1 out of b bits are encoded and the remaining $b - b_1$ are left uncoded. In this case, b_1 coded bits identify one of 2^{b_1} possible subsets of a constellation with 2^b points, where as the $b - b_1$ free bits specify a given point of the selected subsets. The overall spectral efficiency of the considered MLC scheme is $\eta = R \cdot b_1 + (b - b_1)$ [dimension: bits/symbols] [39, 40].

3.2.3 Pilot Symbols and Insertion Loss

Initial synchronization is performed through the insertion of pilot symbols in the transmitted frame, which are known at the receiver. We assume that N_p pilot symbols, with energy E_p, are selected from a 4-QAM constellation and interleaved every N data symbols, thus obtaining the following effective spectral efficiency $\eta' = \eta N/(N+N_p)$. Define $Q \triangleq \frac{N_p E_p}{N E_s}$ as the ratio between the pilot energy and the data symbol energy. The average data symbol energy can be expressed as

$$\bar{E}_s = \frac{N_p E_p + N E_s}{N} = E_s(1+Q)$$

where the factor $(1+Q)$ is the energy penalty due to pilot symbol insertion.

As shown in Figure 3.1, received signal $r(t)$ after front-end filtering is sampled at time instants $\{iT_s\}$. Assuming slowly varying phase noise, the samples $\{r_i\}$[1] can be written as [53]

$$r_i = s_i e^{j\theta_i} + w_i \tag{3.3}$$

with

$$\begin{aligned} s_i &= \sum_{k=-\infty}^{\infty} \tilde{x}_k p[(i-kN_u)T_s] \\ &= \sum_{n=-\infty}^{\infty} x_n p[(i-n)T_s] \end{aligned} \tag{3.4}$$

where the sequence $\{x_n\}$ is obtained by interpolating the sequence $\{\tilde{x}_k\}$ with zeros, i.e.,

$$x_n = \begin{cases} \tilde{x}_{\lfloor \frac{n}{N_u} \rfloor} & n \bmod N_u = 0 \\ 0 & \text{otherwise} \end{cases}$$

in which $\lfloor \cdot \rfloor$ denotes the largest integer less than or equal to the argument. Expression (3.3) can be rewritten as

$$r_i = \sum_{n=-\infty}^{\infty} x_{i-n} p_n e^{j\theta_i} + w_i. \tag{3.5}$$

[1] In this chapter, the subscript k will be used for symbol time and i for sample time, unless otherwise stated.

Although the SRRC filter $\{p_n\}$ has (theoretically) infinite length, it can assumed to be of finite length due to memory and energy constraints, as suggested in [64]. In particular, we consider the most significant L terms, with $L = 2v+1$, so that

$$p_i \simeq \begin{cases} p(iT_s) & \text{if } -v \leq i \leq v \\ 0 & \text{otherwise.} \end{cases} \tag{3.6}$$

Therefore, $2v$ is the number ISI taps of the equivalent filter. Expression (3.5) for the received sample can be approximated as follows:

$$r_i \cong \sum_{n=-v}^{v} x_{i-n} p_n e^{j\theta_i} + w_i. \tag{3.7}$$

The discrete-time phase noise in (3.7) can be described as first-order Markov, where

$$\theta_i = [\theta_{i-1} + \delta_i] \mod 2\pi \tag{3.8}$$

with i.i.d increments $\delta_i \sim \mathcal{N}(0, \sigma_\delta^2)$, being $\sigma_\delta^2 = 2\pi B_\theta T_s$ the variance of the phase noise process at sample time. Using the model (3.8), the phase noise process at symbol rate T can be similarly described as

$$\theta_k = [\theta_{k-1} + \Delta_k] \mod 2\pi$$

where $\Delta_k \sim \mathcal{N}(0, \sigma_\Delta^2)$, with $\sigma_\Delta^2 = N_u \sigma_\delta^2 = 2\pi B_\theta T$.

The received signal (3.7) after pulse shape matched-filtering can be represented as

$$\begin{aligned} \tilde{r}_i &= r_i \otimes p_{-L}^* = \left[\sum_{n=-v}^{v} x_{i-n} p_n e^{j\theta_i} + w_i \right] \otimes p_{-L}^* \\ &= x_i g_L e^{j\theta_i} + \tilde{w}_i \end{aligned} \tag{3.9}$$

given $\tilde{w}_i = w_i \otimes p_{-L}^*$ is an AWGN process with variance $\sigma_{w,Nu}^2 = \frac{N_0}{2} \cdot N_u$ and $g_L = p_L \otimes p_{-L}^*$. Note that up-sampling with a factor N_u of a discrete-time Wiener process $\{\theta_i\}$ leads to an $\sigma_\delta^2 = \sigma_\Delta^2 / N_u$. Similar effect happens for an AWGN channel, such that $\sigma_{w,Nu}^2 = \sigma_{w,1}^2 N_u$, in order to have the same values of the PSD of the noise process as the up-sampling a signal widens the frequency domain without aliasing [65, 66].

Under the assumption of slowly varying phase noise and optimal matched filtering, the traditional receiver considers sampling at kT_s, so that the sampled sequence can be expressed as follows:

$$\tilde{r}_k = x_k e^{j\theta_k} + \tilde{w}_k \tag{3.10}$$

which is a commonly used system model for symbol-time phase noise estimation. In the presence of optimal matched filtering, it would hold that $x_k \simeq \tilde{x}_k$. The average received energy per information bit is $\bar{E}_s/\eta$ and the per-bit SNR γ_b can be finally defined as follows:

$$\gamma_b \triangleq \frac{E_b}{N_o} = \frac{\bar{E}_s}{N_o}\frac{1}{\eta} = \frac{E_s}{N_o}\frac{1+Q}{\eta}.$$

3.3 Phase Synchronization and Detection in a Multi-Sample Receiver

We now recall the approach proposed in Section 2.2 from Chapter 2, for phase synchronization. An accurate phase estimation algorithm should track the phase variations on a sample-by-sample basis. We preliminarily assume that the phase noise process can be approximated as quasi-constant over a (sufficiently short) observation window of ℓ consecutive samples. This assumption leads to block-wise phase noise estimation.

We focus on disjoint consecutive windows, where the phase estimated on a block of length ℓ is used to compensate the phase rotation over all the samples of the same block, which is referred to as block window (see Section 2.2 for detail). Denote as $\hat{\theta}^{(q)}$ the phase estimate over the q-th ℓ-sample block,

$$\hat{\theta}_i = \hat{\theta}^{(q)} \quad i = (q-1)\ell+1,\ldots,q\ell \quad q = 1,2,\ldots,n_p$$

where n_p is the number of disjoint blocks with length ℓ within the same codeword. Denoting the ℓ received observables in the q-th block as $\boldsymbol{r}^{(q)} \triangleq \left[r_{(q-1)\ell+1},\ldots,r_{q\ell}\right]$, under the assumption of constant phase over this block, its ML estimate can be written

as follows:[2]

$$\hat{\theta}_{ML}^{(q)} = \underset{\vartheta\in(0,2\pi)}{\arg\max}\, p(\boldsymbol{r}^{(q)}|\vartheta)$$

Note that, by straightforward application of the Bayes rule, the ML estimate is equivalent to the MAP estimate $\hat{\theta}^{(q)} \triangleq \text{argmax}_{\vartheta\in(0,2\pi)}\, p(\vartheta|\boldsymbol{r}^{(q)})$. The pulse shape and its parameters (namely: roll-off β, filter length L, and oversampling factor N_u) are known at the receiver, so that the sampled signal (3.7) is deterministic but unknown. Let $\boldsymbol{s}_i = \sum_{n=-v}^{v} x_{i-n}p_n$ be the total transmitted signal at the i-th instant.

Strategy 1

Considering the available APPs from the coded symbols $\{\tilde{x}_k\}$ as useful information, the following modified ML strategy can be considered:

$$\hat{\theta}^{(q)} = \underset{\vartheta\in(0,2\pi)}{\arg\max} \sum_{\boldsymbol{s}\in\mathscr{X}^{\ell}} \underbrace{p(\boldsymbol{r}^{(q)}|\vartheta,\boldsymbol{s}^{(q)})}_{\text{Known}} \underbrace{P(\boldsymbol{s}^{(q)}|\boldsymbol{r})}_{\text{From channel dec.}}$$

where: $\boldsymbol{s} \triangleq \left[s_{(q-1)\ell+1},\ldots,\boldsymbol{s}_{q\ell}\right]$; $s_i (i=(q-1)\ell+1,\ldots,q\ell)$, denotes a sample at epoch i drawn from the transmitted signal set $\mathscr{X}$ with $|\mathscr{X}| = M^L$; and $\boldsymbol{r}$ is the entire sequence of received samples, i.e., $\boldsymbol{r} \triangleq \left[\boldsymbol{r}^{(1)},\ldots,\boldsymbol{r}^{(n_p)}\right]$ over which the phase noise estimation is to be performed. The PDF $p(\boldsymbol{r}^{(q)}|\vartheta,\boldsymbol{s}^{(q)})$ is known to be Gaussian from the considered channel model (3.3), where the term $P(\boldsymbol{s}^{(q)}|\boldsymbol{r})$ can be referred to as APP of the unknown constellation which can be calculated based on the filter characteristic and modulation as suggested in [57]. Since we rely on APPs from channel coding, we use $P(\tilde{\boldsymbol{x}}|\boldsymbol{r})$, resulting in an approximate way to estimate phase noise.

In the presence of a channel coding which generates soft outputs in terms of bit Log-Likelihood Ratios (LLRs), the APPs can be obtained directly from the bit LLRs, by taking into account the modulation strategy. Using a derivation similar to that in Section 2.2, the phase estimate for the i-th sample in the q-th block, with $i=(q-1)\ell+1,\ldots,q\ell$, can be expressed as:

$$\hat{\theta}_i = \arg[\Phi_{q\ell,\ell}] \tag{3.11}$$

[2]Lower case letter denotes a probability density function (PDF) and upper case letter denotes a probability.

where

$$\Phi_{q\ell,\ell} \triangleq \left[\sum_{l=0}^{\ell-1} r_{q\ell-l}\alpha^*_{q\ell-l}\right] \tag{3.12}$$

$$\alpha_i \triangleq \sum_{n=-v}^{v} \tilde{\alpha}_{i-n}p_n \tag{3.13}$$

$$\tilde{\alpha}_i = \begin{cases} \tilde{\alpha}_{\lfloor \frac{i}{N_u} \rfloor} & i \bmod N_u = 0 \\ 0 & \text{otherwise.} \end{cases} \tag{3.14}$$

Note that the sequence $\{\tilde{\alpha}_i\}$ is obtained by interpolating the sequence $\{\tilde{\alpha}_k\}$ with zeros as shown in (3.14). The quantity α_i is an (approximate) transmitted sample.

ISI at the received observable is reduced by matched filtering (3.9) followed by symbol-time processing (as shown in the dotted section of Figure 3.4), to obtain reliable soft-information, and consequently, $\{\alpha_i\}$. Note that one sample per symbol is sufficient for sequence detection [63]. The determined APPs from the demapper/SISO decoder values on the bits are considered for soft QAM symbol calculation accordingly as follows:

$$\begin{aligned} \tilde{\alpha}_k &\triangleq \sum_{m=0}^{M-1} p_m^{(k)}\tilde{x}(m) \\ p_m^{(k)} &\triangleq P(\tilde{x}_k = \tilde{x}(m)|\tilde{r}). \end{aligned} \tag{3.15}$$

If a given symbol $\tilde{x}(m)$ has probability close to 1 at any instant k, i.e., $p_m^{(k)} = 1$, then $\tilde{\alpha}_k \simeq \tilde{x}(m)$; on the other hand, if no APP is available, then $\tilde{\alpha}_k$ corresponds to the unweighted center of the constellation. In the presence of a pilot symbol $\tilde{x}_k$, then $\tilde{\alpha}_k = \tilde{x}_k$.

The computation of the probabilities $\{p_m^{(k)}\}$, obtained from the soft-output information generated by the decoder is independent of the presence/absence of MLC [51]. Since an M-ary symbol $\tilde{x}_k$ is labeled by $b = \log_2 M$ bits $(c_k^{(1)}, \ldots, c_k^{(b)})$, one obtains

$$P(\tilde{x}_k|\tilde{\boldsymbol{r}}) = \prod_{j=1}^{\log_2 M} P(c_k^{(j)}|\tilde{\boldsymbol{r}}) = \prod_{j=1}^{\log_2 M} \frac{e^{(1-c_k^{(j)})}\mathscr{L}(c_k^{(j)})}{1+e^{\mathscr{L}(c_k^{(j)})}}$$

where

$$\mathscr{L}(c_k^{(j)}|\tilde{\boldsymbol{r}}) \triangleq \ln \frac{P(c_k^{(j)}=0|\tilde{\boldsymbol{r}})}{P(c_k^{(j)}=1|\tilde{\boldsymbol{r}})}, \qquad j=1,\ldots,\log_2 M$$

are the LLRs output either by the soft-output channel decoder (coded bits) or by the soft-output demapper (free-bits) depending on the MLC-based strategy. Soft QAM symbol (after up-sampling) with pulse shape are used block-wise to determine the phase noise.

As already proposed in Section 2.2.3, we can rely on block window phase estimation scheme based on Phasor Linear Prediction (PLP). According to this approach, the phase estimate (at sample time) is given by

$$\hat{\theta}_{i,\mathrm{ISC}_1} = \arg\left[\sum_{q=0}^{\ell-l} \Phi_{i+q,\ell}\right] \tag{3.16}$$

where

$$\sum_{q=0}^{\ell-l} \Phi_{i+q,\ell} \quad = \quad \sum_{j=-\ell+1}^{\ell-1} u_j r_{i-j} \alpha_{i-j}^{*} \tag{3.17}$$

where $u_j \triangleq \ell - |j|, j \in \{-\ell+1,\ldots,\ell-1\}$. In particular, in (3.17) the weighing coefficients $\{u_j\}$ have a triangular shape. Due to the nature of received observable $\{r_i\}$, we refer this approach to as an Inter-Symbol Correlated (ISC). [3]

Strategy 2

An adaptive filter approach can be employed for matched filtering and noise cancellation [61, 67]. In particular, we consider two sub-adaptive filters to mimic a desired filter response, which can optimize the performance of the receiver in the presence of phase noise.

In the strategy 1, the received observable $\tilde{r}_i$ is used for symbol-time processing in (3.15). In fact, the received observable from the channel consists of a vector $\boldsymbol{r}_i = [r_i\ r_{i+1}\ \ldots\ r_{i+L-1}]^T$, containing $L = 2\nu+1$[4] received samples as an input to the

[3] The subscript in ISC_1 refers to strategy 1 and vice versa.

[4] The L is solely used to avoid any further confusion in the derivation.

matched filter. The $L-1$ additional partial information in the past and future terms in the received observable $\boldsymbol{r}_i$, can be used for phase noise estimation. Note that SRRC filter has a linear-phase response. The output of the matched filter (previously discussed in (3.9), now in terms of L) $\tilde{r}_i$ can be expressed as follows:

$$\tilde{r}_i \;=\; \sum_{l=0}^{L-1} \psi_l r_{i+L-1-l} = \sum_{l=0}^{L-1} p_l^* r_{i+l} \tag{3.18}$$

where $\psi_l = p^*_{L-1-l}, 0 \leq l \leq L-1$ is the impulse response of the matched filter.

For convenience in deriving the proposed phase noise estimation algorithm and making distinction with $\tilde{r}_i$, we assume a vector $\boldsymbol{z}_i$ (an equivalent to $\tilde{r}_i$), such that

$$\boldsymbol{z}_i \triangleq [z_{i-M_2} \;\ldots\; z_{i-1}\; z_i\; z_{i+1} \;\ldots\; z_{i+M_1}] \tag{3.19}$$

The samples $\{z_i\}$, its preceding M_2 samples and subsequent M_1 samples constitutes the vector $\boldsymbol{z}_i$, having length $M_{wd} = M_1 + M_2 + 1$. In addition to L samples of the $\boldsymbol{r}_i$ at the input of the matched filter, an additional M_{wd} samples are required to avoid any non-linearity in (3.19), which can be expressed as follows:

$$\boldsymbol{r}_i \triangleq [r_{i-M_2} \;\ldots\; r_{i-1}\; r_i\; r_{i+1} \;\ldots\; r_{i-M_1+L-1}]^T \tag{3.20}$$

We define a feedforward (i.e., matched filter) filter matrix Ψ of size $M_{wd} \times (M_{wd} + L-2)$ as

$$\Psi = \begin{pmatrix} p_0^* & p_1^* & \cdots & p_{L-1}^* & 0 & \ldots & 0 \\ 0 & p_0^* & p_1^* & \cdots & p_{L-1}^* & 0 & \\ \vdots & \vdots & \ddots & \ddots & \ddots & \ddots & \vdots \\ 0 & 0 & \ldots & p_0^* & p_1^* & \cdots & p_{L-1}^* \end{pmatrix}. \tag{3.21}$$

Based on the (3.18), we obtain

$$\boldsymbol{z}_i = \boldsymbol{r}_i \Psi. \tag{3.22}$$

The decision feedback matrix Ψ_{FB} can be obtained according to (3.9). The matrix Ψ_{FB} has same dimension as Ψ, i.e., $M_{wd} \times (M_{wd} + L - 2)$. Instead ψ_l, we use $g_L =$

$p_L \otimes p^*_{-L}$ as mentioned in (3.9), which can be expressed as follows:

$$\Psi_{\mathrm{FB}} = \begin{pmatrix} g_0 & g_1 & \cdots & g_{L-1} & 0 & \cdots & 0 \\ 0 & g_0 & g_1 & \cdots & g_{L-1} & 0 & \\ \vdots & \vdots & \ddots & \ddots & \ddots & \ddots & \vdots \\ 0 & 0 & \cdots & g_0 & g_1 & \cdots & g_{L-1} \end{pmatrix} \tag{3.23}$$

The symbol-time processed information from (3.13) in conjunction with (3.23) can be used to obtain $\boldsymbol{A}_i$,

$$\boldsymbol{A}_i = \boldsymbol{\alpha}_i \Psi_{\mathrm{FB}}. \tag{3.24}$$

Finally, phase estimate for the i-th sample in the q-th block for a given L-th column can be determined from (3.22) and (3.24), which can be expressed as follows:

$$\sum_{q=0}^{\ell-l} \Phi_{i+q,L} = \sum_{j=-\ell+1}^{\ell-1} u_j \boldsymbol{z}_{i-j} (A_{i-j})^{\dagger} \tag{3.25}$$

$$\hat{\vartheta}_{i,L} = \arg\left[\sum_{q=0}^{\ell-1} \Phi_{i+q,L}\right] \tag{3.26}$$

$$\hat{\theta}_{i,ISC_2} = \frac{1}{L} \sum_{n=1}^{L} \hat{\vartheta}_{i,n} \tag{3.27}$$

where $u_j \triangleq \ell - |j|, j \in \{-\ell+1, \ldots, \ell-1\}$ and $(\cdot)^{\dagger}$ denotes the transpose conjugation of the selected vector set. An average of the estimated L phases in (3.26) are used in (3.27) for each i-th received sample.

3.4 Iterative Receiver Structure

Figure 3.4 shows the proposed low-complexity iterative receiver structure, whose phase estimation is performed at sample time. We now describe the principle of operation of the proposed iterative receiver structure, which consists of matched filtering (MF), linear interpolator (INT), demapper and soft-input soft-output (DEM/SISO) decoder block which consists of demodulation, channel and an MLC decoder. The obtained symbol from the soft-information of the DEM/SISO with known transmit

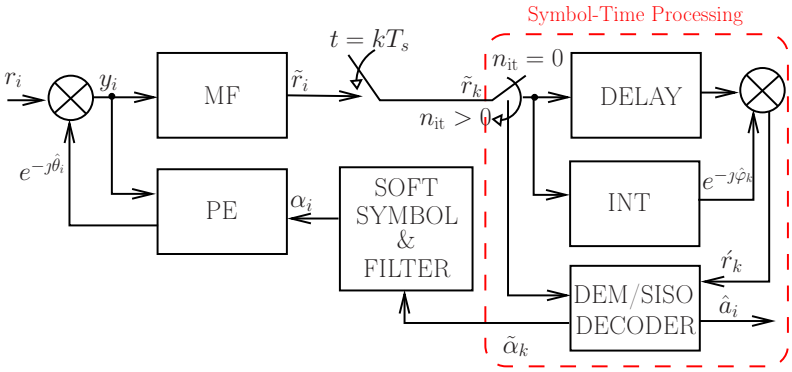

Figure 3.4: Block diagram of the proposed iterative multi-sample receiver.

pulse shape is used in the phase estimation procedure according to (3.16) and (3.27), to perform synchronization at sample instant.

Initially, matched filtering is used to reduce ISI and obtain reliable $\{\tilde{r}_i\}$, which are then fed to symbol-time processing after downsampling with a factor N_u. Linear interpolator would be operational during the first iteration of the iterative receiver and rest of the iteration uses the $\{\tilde{r}_i\}$ directly for the detection. This preliminary phase noise estimation enables the soft demapper and decoder to provide reliable output, which is necessary to perform the remaining iterations of the proposed iterative receiver.

The linear interpolator operates on the known consecutive pilot symbols, which are interleaved in the transmitted data sequence. In correspondence to pilot symbols, the phase noise process is estimated as the difference between the phase of the received symbol and the phase of the transmitted symbol $\tilde{x}_k$:

$$\hat{\theta}_k = \angle \tilde{r}_k \tilde{x}_k^*.$$

The observable at the output of the interpolator, denoted as $\{\acute{r}_k\}$, can be expressed as follows:

$$\acute{r}_k = \tilde{r}_k e^{-\hat{\varphi}_{k,\text{int}}} = \tilde{x}_k e^{-(\theta_k - \hat{\varphi}_{k,\text{int}})} + \tilde{w}_k$$

where $e^{-\hat{\theta}_{k,\text{int}}}$ is the derotation introduced by the linear interpolator block and the noise process $\{\tilde{w}_k\}$ is still i.i.d. Gaussian.

After the initial phase noise compensation by the linear interpolator, the observables $\{\acute{r}_k\}$ are fed directly to the input of the DEM/SISO decoder, which uses the demodulator/decoder, whose soft outputs are then passed to the MLC decoder [51]. Since multi-level coding is used, the soft-output information associated with the free bits should be computed according to the multi-level coding scheme in Section **??**. The channel decoder provides soft output information on the coded bits and, therefore, one can compute the most likely coded sequence output by the channel decoder. For $b_1 = 4$ and $b > b_1$, each 4 decided code bits identify a subset associated with a sub-constellation of size $2^b - 4$, corresponding to $b-4$ free bits. At this point, one can compute the soft output on the free bits based on this sub-constellation. The LLRs on the channel coded bits and on the free bits can then be combined to generate APPs on the constellation symbols. The obtained symbol from the soft-information of the DEM/SISO with known transmit pulse shape is used to estimate the phase noise in the transmitted sequence.

After the first iteration, the $\{\tilde{r}_k\}$ will be used for a maximum of n_{it} iterations. At the $\tilde{n}$-th iteration ($\tilde{n} = 1, \ldots, n_{\text{it}}$), the phase estimator operates on the observables vector $\boldsymbol{y}[\tilde{n}]$ obtained as

$$\boldsymbol{y}[\tilde{n}] = \boldsymbol{r} \circ e^{-\hat{\boldsymbol{\theta}}[\tilde{n}-1]} \tag{3.28}$$

where $\boldsymbol{r}$ is the received observable from the channel, and $\hat{\boldsymbol{\theta}}[\tilde{n}-1]$ is the estimated phase noise for a given $\tilde{n}$-th iteration. The symbol $\circ$ represents the Hadamard (or element-wise) product between two vectors. Note that the exponential function is applied element-wise to the vector $\hat{\boldsymbol{\theta}}[\tilde{n}-1]$. The observable $\boldsymbol{y}[\tilde{n}]$ is fed to the DEM/SISO decoder after matched filtering to compute the APPs on the transmitted symbols and to be used in (3.16) or (3.26) for their respective phase estimation algorithm. Note that, since the derotated observable $\boldsymbol{y}[\tilde{n}]$ is used, the estimated phase corresponds to a residual phase error $\hat{\boldsymbol{\vartheta}}[\tilde{n}]$, which is accumulated to obtain the phase estimate

$$\hat{\boldsymbol{\theta}}[\tilde{n}] = \hat{\boldsymbol{\theta}}[\tilde{n}-1] + \hat{\boldsymbol{\vartheta}}[\tilde{n}]$$

to be used in (3.28). After n_{it} iterations, a final decision on the vector of transmitted bits is emitted.

3.5 Performance Analysis

3.5.1 Simulation Setup

In this section, we investigate the performance in terms of BER of the proposed receiver scheme with iterative synchronization and demodulation/decoding for a coded 64-QAM scheme based on MLC strategy. $N_p = 1$ pilot symbol is inserted in the frame every $N = 48$ symbols and belongs to a 4-QAM constellations with average energy 2.5 times the average energy of the data symbols. The channel code is an LDPC code with rate $R = k/n_1 = 7/8$, with $k = 7056$ and $n_1 = 8064$. The exponent parity-check matrix construction (semi-random technique) and the encoding algorithm of the used LDPC code are those of the WiMAX standard [[49], Paragraph 8.4.9.2.5, Annex H]. In particular, the exponent parity-check matrix has $n_{b,r} = 12$ rows, $n_{b,c} = 96$ columns, a spreading factor $Z_f = 84$, a constant row weight $w_r = 32$ and an average column weight $w_c = 4$. LDPC decoding is based here on the sum-product algorithm, where at the end of each internal iteration the algorithm verifies the parity check equation of the code and stops if it is satisfied. The maximum number of decoding iterations are set to 50.

3.5.2 Numerical Results

In Figure 3.5, the BER is shown, as function of γ_b, for 64-QAM, $\sigma_\Delta = 1^\circ$, 5 iterations, and window length $\ell_1 = \ell/N_u = 32$ symbols. In particular, we assume two samples per symbol i.e., $N_u = 2$. A filter with finite length $L = 13$ with a roll-off $\beta = 0.3$ is used to analyzed the performance of the system. The simulation results are compared with traditional receiver structure which assumes only one sample per symbol at the channel and receiver with an optimized phase estimation algorithm i.e., PLP in Section 2.2.3. The traditional receiver is also simulated with more samples per symbol at the channel and one sample per symbol at the receiver. The "PLP with matched filtering" (PLP-MF) considers two samples per symbol at the channel and one sample per symbol at the receiver. The proposed iterative receivers using phase estimation algorithm based on ISC_1 and ISC_2 schemes assumes two samples per symbol at the

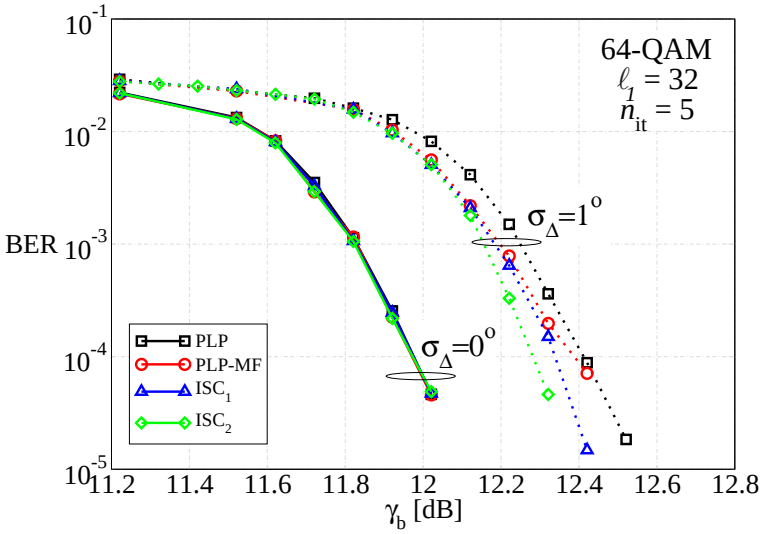

Figure 3.5: BER as a function of γ_b for the proposed receiver with $\beta = 0.3$, $L = 13$, $\sigma_\Delta = 1^\circ$, and $n_{it} = 5$.

channel and receiver. For fair comparison, we assume same filter characteristics i.e., $L = 13$, $\beta = 0.3$.

It can be noticed here from the simulation results in Figure 3.5, that the phase noise model considering one sample per symbol is a “worst-case" scenario. An improvement can be noticed with the PLP-MF which consider two samples per symbol at the channel. The performance of the proposed iterative receiver scheme using ISC_1 and ISC_2 based algorithms performs better than the system with PLP and PLP-MF. Simulation results with ISC_2 are slightly better than ISC_1.

In Figure 3.6, the simulations are repeated for $n_{it} = 10$ with same parameter settings and the performance of receivers with $\sigma_\Delta = 1.5^\circ$ is also included. From the simulation results, we notice that the performance of the proposed iterative receiver achieves better performance at both phase noise variances i.e., $\sigma_\Delta = 1^\circ, 1.5^\circ$.

The performance of the iterative receiver for different values of filter length $L = 2v + 1$, where $v = N_u v_1$ is presented in Figure 3.7. For equal spacing for each L,

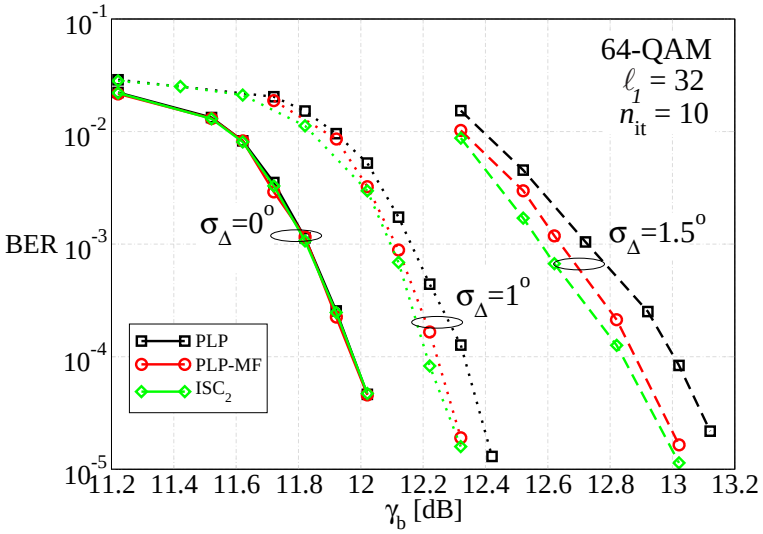

Figure 3.6: BER as a function of γ_b for the proposed receiver with $\beta = 0.3$, $L = 13$ and $n_{it} = 10$. Various values of σ_Δ are considered.

we consider BER as a function of v_1. It can be noticed that the performance of the receiver improves by increasing the value of β and v_1 and window length ℓ for $N_u = 2$ sample per symbol. The improvement due to an increase in the value of β is due to the fact that the ISI reduces with an increase in β value, which improves the receiver performance. Similar analogue holds for $L = 2N_u v_1 + 1$, as an increase in the values of L, better characterizes the ISI. Since the various parameter settings (pilot spacing, coding-rate R, β, N_u etc.) may affect phase noise estimation performance in different ways, the comparisons made here may not be conclusive, and further investigation is a subject of future work.

3.6 Concluding Remarks

In this chapter, we have analyzed the performance of pilot symbol-aided iterative synchronization based on MAP phase estimation for a phase noise-impaired communica-

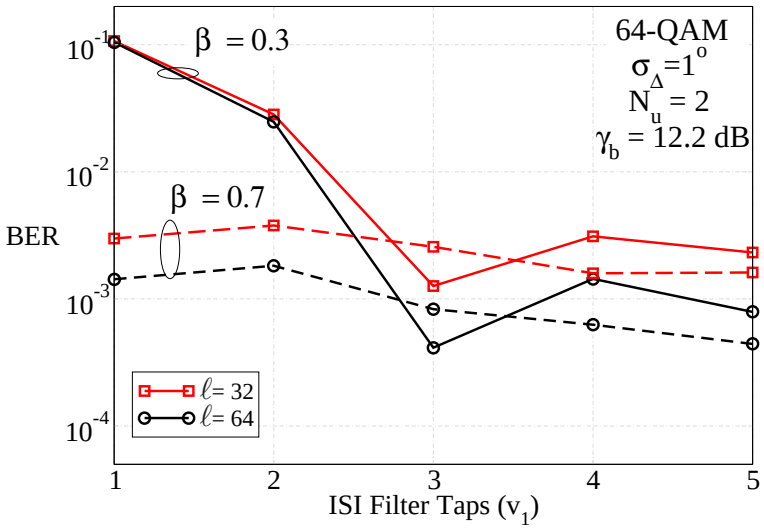

Figure 3.7: Block diagram of the proposed iterative multi-sample receiver.

tion system, where both the channel and the receiver are characterized by more than one sample per symbol interval. We have derived a low-complexity phase synchronization algorithm, which has been exploited in a proper iterative receiver structure. Despite, some work in the literature for multi-sample receiver for phase noise channel from information-theoretic perspective, this work proposes a pragmatic iterative synchronization receiver that exploits more samples per symbol from the channel. Our simulation results with medium constellation e.g., 64-QAM clearly shows the robustness of the proposed receiver.

Chapter 4

Phase Synchronization for Dually-Polarized Communications

Dually-polarized radio schemes are an attractive design choice for future wireless communication systems, as the overall spectral efficiency is directly twice that supported by each component polarization. However, Cross-Polarization Interference (XPI) has a detrimental impact on the system robustness, where phase noise adds further perturbation, making the design of dually-polarized systems challenging.

In this chapter, we propose an innovative Minimum Mean Square Error (MMSE)-based iterative synchronization algorithm for an asynchronous dually-polarized radio link affected by phase noise. A novel soft decision-directed iterative receiver, for separate A Posteriori Probability (APP)-based synchronization and decoding, is proposed. The key idea of the proposed synchronization algorithm relies on an MMSE-based cancellation of the XPI followed by phase estimation on the polarization of interest. An attractive feature of the proposed approach is the fact that it requires no statistical knowledge of the phase noise process.

The rest of this chapter is structured as follows. In Section 4.2, the system model used for the dually-polarized system is presented, where as Section 4.3, we derive the novel phase noise estimation algorithm for the XPD scenario. Section 4.4, we devise an iterative receiver for the proposed strategy. Performance analysis is given

in Section 4.5 and Section 4.6 concludes this chapter.

4.1 Introduction

Antenna polarization diversity provides a cost- and spatial-effective solution to increase spectral efficiency [2]. In the presence of polarization diversity, two independent data streams are transmitted through two orthogonal polarizations (namely, vertical and horizontal polarizations) using the same carrier frequency: these systems are typically referred to as dually-polarized systems. In practice, however, the two polarizations are not perfectly orthogonal. In particular, there can be some energy "leakage" between the polarizations, thus generating Cross-Polarization Interference (XPI). The influence of the XPI is especially noticeable when dual polarization is considered with phase/amplitude modulated schemes, e.g., Quadrature Amplitude Modulation (QAM). As shown in [3, 68], the overall bandwidth efficiency of the microwave radio-link can be improved by using a Cross-Polarization Interference Canceler (XPIC) at the receiver. In remainder of this chapter, dually-polarized systems with the use of an XPIC at the receiver will be referred to as Cross-Polarization Discrimination (XPD) systems.

XPD system is an attractive choice for future wireless communication systems, where carrier synchronization plays a pivotal role. In this context, the radio-frequency oscillators are crucial components in wireless communication transceivers, which are used for the generation of reference signals in the synchronization setup. A realistic oscillator is subject to unwanted noise, in terms of temporal instabilities and spectral dispersions. These instabilities, collectively referred to as phase noise [1], induce distortions (in the limiting case, complete loss of information) in traditional receivers. A vast research literature on phase noise-impaired single polarization transmission schemes exists, from both communication-theoretic and information-theoretic perspectives [9, 11, 12]. However, a very limited portion of the research literature has addressed the carrier synchronization problem in XPD systems. In the presence of spectrally efficient modulations (e.g., high-order QAM) in XPD systems, phase noise becomes detrimental, even in the presence of equalization and XPIC at the receiver.

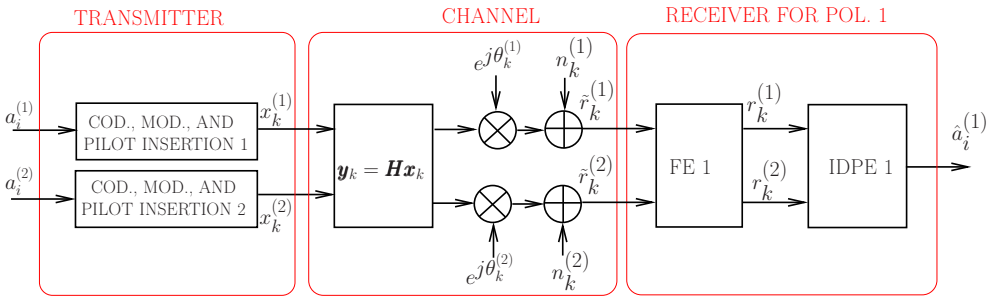

Figure 4.1: Block diagram of the considered XPD system.

In this chapter, a phase noise-impaired XPD system with independent data transmission stream are considered and a novel iterative synchronization/detection receiver structure is proposed. In fact,: (*i*) the transmitters in the two polarization planes are not synchronized (time-wise and phase-wise); and (*ii*) at the receiver side, for each polarization "branch," the corresponding decoder and synchronizer have no direct access to side information (in terms of phase estimates and data decisions) coming from the other polarization branch.

4.2 System Model

The block diagram of the reference system model is shown in Figure 4.1. At the transmitter, two independent binary information sequences $\{\boldsymbol{a}^{(i)}\}_{i=1}^{2}$ are generated at a common bit rate r_{b} (dimension: [b/s]). Each information sequence $\boldsymbol{a}^{(i)}(i=1,2)$ is encoded by a binary channel code, with code rate R, into a coded sequence $\boldsymbol{c}^{(i)}$. Each coded binary sequence is modulated using a modulation scheme with constellation size equal to $M = 2^b$ and average symbol energy E_s.

4.2.1 Multi-Level Coding

Multi-level channel encoding strategy is considered for high-order modulation schemes [37]. More precisely: for small-size constellations (say $b \leq b_1$, where b_1 is a small integer), all bits are encoded; for medium/high-size constellations, i.e., for $b > b_1$, b_1

out of b bits are encoded ("coded" bits) and the remaining $b_2 = b - b_1$ bits are left uncoded ("free" bits).[1] Therefore, in the latter case b_1 coded bits identify one of 2^{b_1} possible subsets of a constellation with a total of 2^b points, whereas the b_2 free bits specify a given point of the selected subset. According to Ungerboeck set partitioning [13], subsets are designed to maximize the Euclidean distance between symbols in each subset. Gray mapping, in terms of free bits, is used to label the points in a given subset [39, 40]. The overall spectral efficiency of the considered multi-level coding scheme is

$$\eta = \begin{cases} R \cdot b \quad \text{bit/symb} & \text{if } b \leq b_1 \\ R \cdot b_1 + (b - b_1) \quad \text{bit/symb} & \text{if } b > b_1. \end{cases}$$

Although the proposed approach is very general (in terms of the considered coded modulation schemes) and, as will be shown in Section 4.3, requires only APPs on the transmitted symbols, in Section 4.5 we will focus on LDPC-coded M-QAM schemes. In particular, no multi-level coding is considered up to 16-QAM (i.e., $b = b_1 = 4$), whereas it is applied to larger constellation sizes (e.g., 64-QAM or 1024-QAM, keeping $b_1 = 4$ in both cases).

4.2.2 Pilot Symbols and Insertion Loss

Initial synchronization (in the absence of APPs) is performed through the insertion, in the transmitted frame, of pilot symbols, known at the receiver, with energy higher than the average energy of data symbols [41]. We assume that N_p pilot symbols are interleaved every N data symbols, thus leading to the following effective spectral efficiency:

$$\eta' = \eta \frac{N}{N + N_\mathrm{p}} \qquad \text{bit/symb.}$$

Denoting the pilot symbol energy as E_p, we define

$$q \triangleq \frac{N_\mathrm{p} E_\mathrm{p}}{N E_\mathrm{s}} \tag{4.1}$$

[1] This approach has the implementation advantage of keeping the coding strategy unalterated even if the modulation order increases.

as the ratio between pilot and data energies. Typically, $q \leq 1$, in fact, if $q > 1$ the system would be inefficient, as more energy would be reserved to pilot symbols rather than to data symbols.

The average data symbol energy can then be expressed as

$$\overline{E}_{\mathrm{s}} = \frac{\text{total frame energy}}{\text{number of data symbols}} = \frac{N_{\mathrm{p}}E_{\mathrm{p}} + NE_{\mathrm{s}}}{N} = E_{\mathrm{s}}(1+q) \tag{4.2}$$

where the factor $(1+q)$ takes into account the energy penalty due to pilot symbol insertion. The average energy per information bit is equal to $\overline{E}_{\mathrm{s}}/\eta$ and the per-bit Signal-to-Noise Ratio (SNR) γ_b can be defined as follows:

$$\gamma_{\mathrm{b}} \triangleq \frac{E_{\mathrm{b}}}{N_0} = \frac{\overline{E}_{\mathrm{s}}}{N_0}\frac{1}{\eta} = \frac{E_{\mathrm{s}}}{N_0}\frac{1+q}{\eta}.$$

4.2.3 XPD Channel and Phase Noise

All oscillation phases (at the transmitters and at the receivers) are assumed to be independent. In this scenario, the overall transmitted sample on the i-th polarization branch can be given the following expression:

$$\tilde{x}_k^{(i)} = h_{ii}x_k^{(i)}e^{j\phi_k^{(i)}} + h_{ij}x_k^{(j)}e^{j\phi_k^{(j)}} \qquad i,j \in \{1,2\} \quad i \neq j \tag{4.3}$$

where: k is the symbol epoch; i/j denote the polarizations (i.e., vertical or horizontal); $x_k^{(i)}/x_k^{(j)}$ are the QAM modulated symbols on the i/j-th polarization associated with the coded symbols $c_k^{(i)}/c_k^{(j)}$; and $\phi_k^{(i)}/\phi_k^{(j)}$ are the phase rotations incurred by symbols $x_k^{(i)}/x_k^{(j)}$ in the two polarization branches at the transmitter. The matrix

$$\boldsymbol{H} \triangleq \begin{bmatrix} h_{11} & h_{12} \\ h_{21} & h_{22} \end{bmatrix}$$

fully characterizes the cross-polarization "intersection" between the two information flows. In particular: h_{ij} $(i,j=1,2,\ i \neq j)$ denotes the interference induced by the j-th polarization transmission on the i-th polarization one (referred to as cross-polar term); whereas h_{ii} $(i=1,2)$ denotes the co-polar gain. In the application of interest,

$|h_{ii}| > |h_{ij}|$ ($j \neq i$), i.e., the interference induced by the signal transmitted on other polarization branch is smaller than the useful signal.

The observable at the input of the receiver relative to the i-th polarization branch can be written as follows:

$$\tilde{r}_k^{(i)} = \tilde{x}_k^{(i)} e^{j\psi_k^{(i)}} + n_k^{(i)} \qquad i \in \{1,2\} \tag{4.4}$$

where: $\tilde{x_k}$ is given by (4.3); $\psi_k^{(i)}$ is the channel-induced phase rotation experienced by the signal in the i-th polarization branch; and $n_k^{(i)}$ is an Additive White Gaussian Noise (AWGN) complex sample with per component variance $\sigma^2 = N_0/2$. Inserting (4.3) in to (4.4) leads to the following expression for the observable:

$$\begin{aligned} \tilde{r}_k^{(i)} &= \left(h_{ii} x_k^{(i)} e^{j\phi_k^{(i)}} + h_{ij} x_k^{(j)} e^{j\phi_k^{(j)}} \right) e^{j\psi_k^{(i)}} + n_k^{(i)} \\ &= h_{ii} x_k^{(i)} e^{j\theta_k^{(ii)}} + h_{ij} x_k^{(j)} e^{j\theta_k^{(ji)}} + n_k^{(i)} \qquad i,j \in \{1,2\} \quad i \neq j \end{aligned} \tag{4.5}$$

where $\theta_k^{(ii)} \triangleq \phi_k^{(i)} + \psi_k^{(i)}$ and $\theta_k^{(ji)} \triangleq \phi_k^{(j)} + \psi_k^{(i)}$. If the two transmitted signals are modulated using the same oscillator,[2] then $\phi_k^{(i)} = \phi_k^{(j)}$ and expression (4.5) reduces to

$$\tilde{r}_k^{(i)} = h_{ii} x_k^{(i)} e^{j\theta_k^{(ii)}} + h_{ij} x_k^{(j)} e^{j\theta_k^{(ii)}} + n_k^{(i)} \qquad i,j \in \{1,2\} \quad i \neq j. \tag{4.6}$$

The phase noise process $\{\theta_k^{(ii)}\}$ is generated according to a proper discrete-time model, which realistically represents (in discrete-time) the experimental (continuous-time) phase noise process affecting the local oscillators at the transmitter. In particular, a phase noise model with quadratic power spectrum decaying is considered for simulation purposes [42]. The equivalent discrete-time model is the well-known Wiener model, which can be given the following general expression:

$$\theta_k = \theta_{k-1} + \Delta_k$$

where $\Delta_k \sim \mathcal{N}(0, \sigma_\Delta^2)$ are independent and identically distributed (i.i.d.) Gaussian increments with zero mean and variance σ_Δ^2. Although we consider a Wiener phase

[2] In general, the two components $\theta_k^{(ii)}$ and $\theta_k^{(ji)}$ have identical statistical distribution. Therefore, expression (4.6) for $\tilde{r}_k^{(i)}$ accurately characterizes the behavior of the XPD systems in the presence of phase noise.

noise model, we remark that our approach is general and can be applied to various phase noise models. In fact, as will be shown later, the proposed synchronization strategy is "blind," as it does not require any a priori statistical knowledge of the phase noise process.

The receiver, as shown in Figure 4.1, is composed by two sub-blocks: the Front End (FE) and the Iterative Detection and Phase Estimation (IDPE) sub-block. In fact, bootstrapping (carried out by the FE sub-block) is required before activation of the iterative synchronization/detection procedure (carried out by the IDPE sub-block). As shown in Figure 4.1, the FE is a preliminary stage which removes the non-linearities present in the received signal $\{\tilde{r}_k^{(i)}\}_{i=1}^2$: the "refined" observables at the input of the IDPE sub-block will be denoted as $\{r_k^{(i)}\}_{i=1}^2$. In Section 4.4, the FE and the IDPE sub-blocks are discussed in detail. As shown in Figure 4.1, the IDPE sub-block is composed by a soft-output demodulation/decoding block (which will be "off-the-shelf") and a phase estimation block, where a novel MMSE-based XPI cancellation and phase estimation algorithm, which exploits APPs generated by the soft-output demodulator/decoder is used. Section 4.3 is dedicated to preliminary derive this algorithm.

4.3 MMSE-based XPI cancellation and Synchronization

With the aim of keeping the computational complexity low, inspired by the work in [44] for channels affected by a constant phase offset, we preliminarily assume that the phase noise process can be approximated as quasi-constant over a (sufficiently short) observation window of ℓ consecutive samples. This assumption leads naturally to block-wise XPI cancellation and phase noise estimation. In particular, the window length ℓ should be chosen as a tradeoff: it should be as small as possible to meet the quasi-constant assumption of the phase noise, but it should also be as large as possible to average out the negative impact of the AWGN.

Unlike "classical" phase estimation in single polarization systems, in dually-polarized systems XPI has to be carefully taken in to account. Our approach will aim at canceling XPI before carrying out phase estimation for the polarization of interest.

In Subsection 4.3.1, we first focus on disjoint consecutive windows, where, through an MMSE-based strategy, the phases estimated (on both polarizations) for a block of length ℓ is used to cancel the XPI and then compensate the phase rotations over all symbols of the same block: this approach is referred to as Block Window (BW). In Subsection 4.3.2, a sliding window phase estimation strategy is then derived as an extension of the BW strategy.

4.3.1 Block Window

MMSE Strategy *with* Perfect Symbol Knowledge

The BW MMSE XPI cancellation and phase estimation strategy is motivated from the Master/Slave phase synchronized first-order Phase-Locked Loop (PLL) scheme proposed in [69]. The operational principle of a Master/Slave Phase Estimation (M/S-PE) block is to improve the phase tracking performance of both polarization branches: more precisely, the M-PE block is the starting one and the S-PE block exploits the phase estimated by the former. In the considered XPD system, the M-PE block is associated with the branch of interest (referred to as co-polar branch).

We preliminary denote the m-th ℓ-symbol block of observables on the i-th ($i \in \{i,2\}$) polarization branch as:

$$\boldsymbol{r}_m^{(i)} \triangleq [r_{(m-1)\ell+1}^{(i)}, \ldots, r_{m\ell}^{(i)}], \qquad m = 1,2,\ldots,n_{\mathrm{p}}$$

where n_{p} is the number of ℓ-symbol disjoint blocks within the same codeword.[3] As anticipated above, we assume that, over a window of length ℓ, the estimated phase process $\{\hat{\varphi}_k^{(i)}\}_{k=(m-1)\ell+1}^{m\ell}$ over the ℓ symbols of the m-th block can be approximated as constant, i.e.:

$$\hat{\varphi}_k^{(i)} = \hat{\varphi}_m^{(i)} \qquad k = (m-1)\ell+1,\ldots,m\ell \quad i \in \{1,2\}.$$

The overall phase estimate vector over the symbols associated with a particular codeword is denoted as $\hat{\boldsymbol{\varphi}}^{(i)} \triangleq [\hat{\varphi}_{(1)}^{(i)}, \ldots, \hat{\varphi}_{(n_{\mathrm{p}})}^{(i)}]$.

[3] In the following, we will use the subscript k for the symbol index and bold symbols with the subscript m for the the m-th block.

Given the above assumptions and assuming perfect knowledge of the co-polar symbols $\{x_k^{(1)}\}_{k=(m-1)\ell+1}^{m\ell}$, the proposed BW estimation strategy reads as follows:

$$\hat{\varphi}_m^{(1)}, \hat{\varphi}_m^{(2)} = \underset{\varphi_m^{(1)}, \varphi_m^{(2)}}{\operatorname{argmin}} \sum_{l=0}^{\ell-1} \left| \tilde{z}_{m\ell-l}^{(1)} - x_{m\ell-l}^{(1)} \right|^2 \tag{4.7}$$

where

$$\tilde{z}_{m\ell-l}^{(1)} \triangleq \left[r_{m\ell-l}^{(1)} + r_{m\ell-l}^{(2)} e^{-\varphi_m^{(2)}} \right] e^{-\varphi_m^{(1)}}. \tag{4.8}$$

The intuitive idea behind the block-wise MMSE strategy in (4.7) is that of using the modified observables $\{\tilde{z}_{m\ell-l}^{(1)}\}$, as defined in (4.8), which are obtained from the co-polar branch observables $\{r_{m\ell-l}^{(1)}\}$ by first eliminating the XPI and then, by de-rotating the "cleaner" observable. Using (4.8) into (4.7) and dropping irrelevant terms, after a few simple manipulations, one obtains:

$$\begin{aligned} \hat{\varphi}_m^{(1)}, \hat{\varphi}_m^{(2)} &= \underset{\varphi_m^{(1)}, \varphi_m^{(2)}}{\operatorname{argmin}} \sum_{l=0}^{\ell-1} \left[\left| \tilde{z}_{m\ell-l}^{(1)} \right|^2 - 2\Re \left\{ \tilde{z}_{m\ell-l}^{(1)} \left(x_{m\ell-l}^{(1)} \right)^* \right\} + \left| x_{m\ell-l}^{(1)} \right|^2 \right] \\ &= \underset{\varphi_m^{(1)}, \varphi_m^{(2)}}{\operatorname{argmax}} \Re \left\{ B e^{-\varphi_m^{(1)}} + C e^{-(\varphi_m^{(1)} + \varphi_m^{(2)})} + D e^{-\varphi_m^{(2)}} \right\} \end{aligned} \tag{4.9}$$

where

$$B \triangleq \textstyle\sum_{l=0}^{\ell-1} r_{m\ell-l}^{(1)} (x_{m\ell-l}^{(1)})^* \tag{4.10}$$

$$C \triangleq \textstyle\sum_{l=0}^{\ell-1} r_{m\ell-l}^{(2)} (x_{m\ell-l}^{(1)})^* \tag{4.11}$$

$$D \triangleq -\textstyle\sum_{l=0}^{\ell-1} r_{m\ell-l}^{(2)} (r_{m\ell-l}^{(1)})^*. \tag{4.12}$$

From (4.9), given $\varphi_m^{(2)}$, it would follow that

$$\hat{\varphi}_m^{(1)} = \arg \left[B + C e^{-\varphi_m^{(2)}} \right]. \tag{4.13}$$

Similarly, given $\varphi_m^{(1)}$, from (4.9) it would follow that

$$\hat{\varphi}_m^{(2)} = \arg \left[D + C e^{-\varphi_m^{(1)}} \right]. \tag{4.14}$$

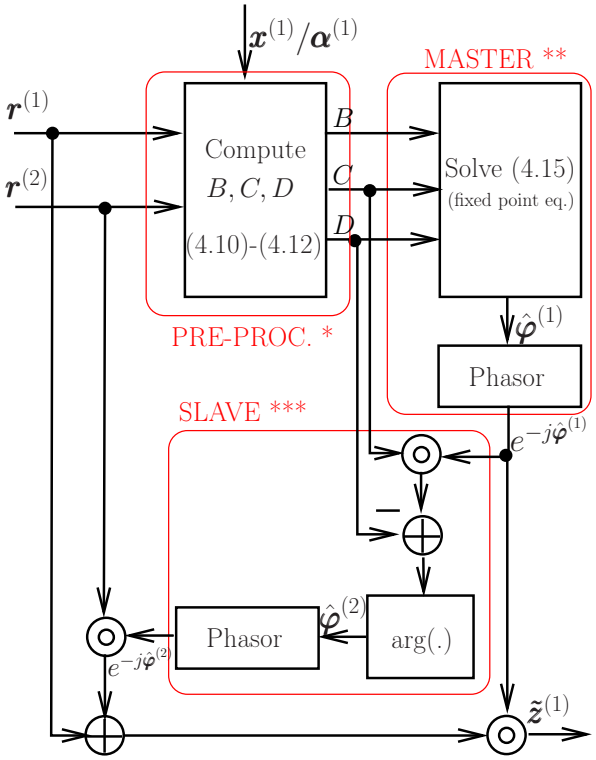

Figure 4.2: Block diagram of the proposed Master/Slave synchronization scheme (i.e., equations (4.15) and (4.16)). The observable sequence $\boldsymbol{r}^{(1)}$ corresponds to the polarization of interest.

Under the assumption (verified later) that a unique solution $(\hat{\varphi}_m^{(1)}, \hat{\varphi}_m^{(2)})$ exists, inserting (4.14) into (4.13) one obtains

$$\hat{\varphi}_m^{(1)} \quad \text{s. t.} \quad \hat{\varphi}_m^{(1)} = \underbrace{\arg\left[B + Ce^{-\arg\left[D+Ce^{-\hat{\varphi}_m^{(1)}}\right]}\right]}_{\triangleq f(\hat{\varphi}_m^{(1)})} \tag{4.15}$$

$$\hat{\varphi}_m^{(2)} = \arg\left[D + Ce^{-\hat{\varphi}_m^{(1)}}\right]. \tag{4.16}$$

In Figure 4.2, block diagram of the M/S-PE scheme corresponding to (4.15) and

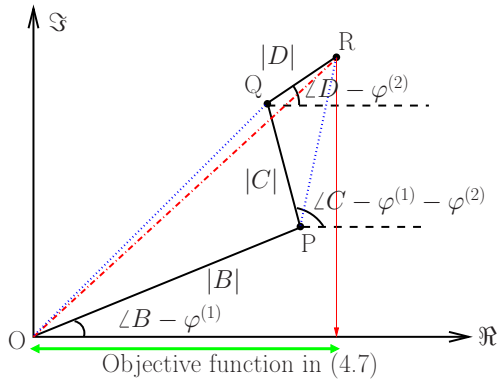

(a)

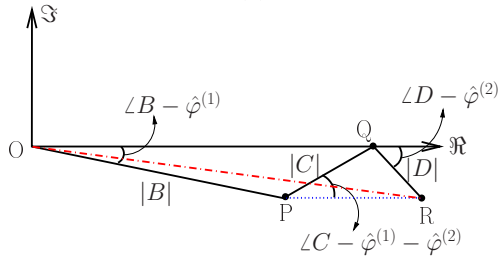

(b)

Figure 4.3: Geometric interpretation of the optimization problem in (4.9): (a) general geometric setting and (b) optimal MMSE solution.

(4.16) is shown. In Figure 4.3, a geometric interpretation of the optimization problem in (4.9) is shown, for simplicity, the block index m has been dropped. In particular, in Figure 4.3 (a) the general geometric setting is shown, with the explicit indication of the three segments which correspond to the three addenda inside the real operator at the right-hand side of (4.9). The complex argument of the real operator is denoted as R. The maximization problem in (4.9) is equivalent to selecting the two angles $\varphi^{(1)}$ and $\varphi^{(2)}$ so that the real part of the complex number R or, equivalently, the real part of the segment $\overline{\mathrm{OR}}$ is maximized. It can be geometrically shown, as illustrated in Figure 4.3 (b), that the real part of the segment $\overline{\mathrm{OR}}$ is maximum when the segments $\overline{\mathrm{OQ}}$ and $\overline{\mathrm{PR}}$ are parallel to the real axis (in particular, the segment $\overline{\mathrm{OQ}}$ lies on the real

axis). This can be intuitively explained as follows:

- first, by varying the angle $\varphi^{(1)}$, it is possible to bring the point Q on the real axis: this is the "best" strategy to maximize the real part of the segment $\overline{\mathrm{OR}}$ by acting only on $\varphi^{(1)}$;
- at this point, by varying the angle $\varphi^{(2)}$, the the real part of the segment $\overline{\mathrm{OR}}$ is maximized when the segment $\overline{\mathrm{PR}}$ is parallel to the real axis;
- the second step of the geometric optimization procedure might have moved the point Q off the real axis: if so, then the angle $\varphi^{(1)}$ can be further readjusted in order to bring Q on the real axis and to further maximize the real part of the segment $\overline{\mathrm{OR}}$;
- at this point, $\varphi^{(2)}$ and $\varphi^{(1)}$ are recursively adjusted (with minor and minor variations) in order to reach the configuration in Figure 4.3 (b). The corresponding final phases $\hat{\varphi}^{(1)}$ and $\hat{\varphi}^{(2)}$ are the phase estimates obtained according to the proposed MMSE strategy and composed to (4.15) and (4.16).

Although the above geometric considerations show that the solution $(\hat{\varphi}^{(1)}, \hat{\varphi}^{(2)})$ is unique, a rigorous mathematical proof is an open research problem. Note that (4.15) is a fixed-point equation, whose solution can be obtained by leveraging on any iterative algorithm suited to solve this kind of problem. In Figure 4.4, $\varphi_m^{(1)}$ and $f(\varphi_m^{(1)})$, which appears in (4.15), are shown in radians. One should observe that $f(\varphi_m^{(1)})$ is a periodic function of $\varphi_m^{(1)}$ and a unique intersection with the line $\varphi_m^{(1)}$ exists. Therefore, the function $f(\varphi_m^{(1)}) - \varphi_m^{(1)}$ has only one zero, which corresponds to the unique solution of (4.15).

Based on (4.13), the phase estimate for the k-th symbol in the m-th block ($k = (m-1)\ell + 1, \ldots, m\ell$) can finally be expressed as

$$\hat{\varphi}_{k,\mathrm{BW}}^{(1)} = \arg\left[B + Ce^{-\varphi_m^{(2)}}\right] = \arg[\Phi_{ml,l}^{\mathrm{APP}_1}] \tag{4.17}$$

where the subscript BW has been introduced to clearly refer to the BW strategy and,

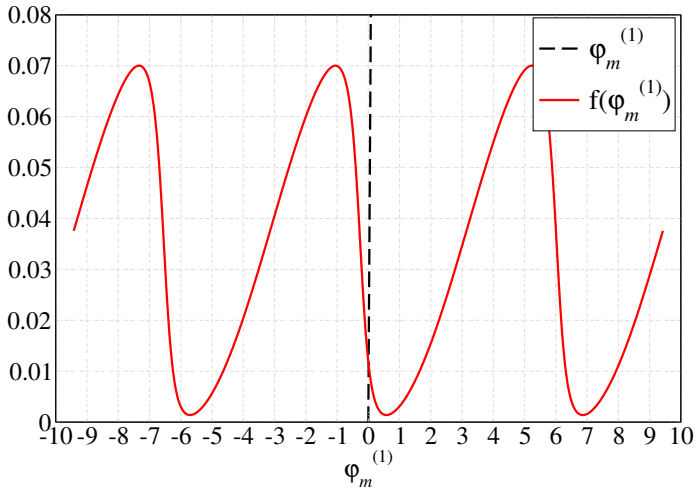

Figure 4.4: $\varphi_m^{(1)}$ and $f(\varphi_m^{(1)})$ (as defined in (4.15)) in radians, for 64-QAM modulation, $\gamma_b = 12.5$ dB and $\ell = 16$.

from the definitions of B and C in (4.10) and (4.11),

$$\Phi_{ml,l}^{\text{APP}_1} \triangleq \sum_{l=0}^{\ell-1} \left[r_{m\ell-l}^{(1)} (x_{m\ell-l}^{(1)})^* + r_{m\ell-l}^{(2)} (x_{m\ell-l}^{(1)})^* e^{-\varphi_m^{(2)}} \right]. \tag{4.18}$$

Similarly, from C and D defined in (4.11) and (4.12), expression (4.14) can be equivalently written as:

$$\hat{\varphi}_{k,\text{BW}}^{(2)} = \arg[\Phi_{ml,l}^{\text{APP}_2}] \triangleq \arg \sum_{l=0}^{\ell-1} \left[r_{m\ell-l}^{(2)} (x_{m\ell-l}^{(1)})^* e^{-\varphi_m^{(1)}} - r_{m\ell-l}^{(2)} (r_{m\ell-l}^{(1)})^* \right]. \tag{4.19}$$

MMSE Strategy *with* APPs

From a practical point of view, perfect knowledge of the co-polar symbols $\{x_{m\ell-l}^{(1)}\}$ is impossible. In practice, provided that a prior soft information on $\{x_{m\ell-l}^{(1)}\}$ is available, then a symbol $x_{m\ell-l}^{(1)}$ can be replaced by the following "soft symbol" based on available symbol APPs $\{p_{lm}\}$:

$$\alpha_{m\ell-l}^{(1)} \triangleq \sum_{m_1=0}^{M-1} p_{lm} \tilde{x}^{(m_1)}$$

where $\{\tilde{x}^{(m_1)}\}_{m_1=0}^{M-1}$ are symbols of the considered modulation constellations. In other words, $\alpha_{m\ell-l}$ represents the *center of gravity* of the transmitted constellation, at time instant $m\ell-l$, based on the symbol APPs. For example, in the presence of channel coding, $\{p_{lm}\}$ can be derive from a soft-output decoder, as we now consider.

The symbol APPs $\{p_{lm}\}$ are computed from the bit APPs output by the channel decoder. With reference to the channel coding scheme introduced in Section 4.2, we remark that the detection of the symbol APPs is independent of the presence/absence of the multi-level coding strategy. In fact, if multi-level coding is not considered (i.e., $b_1 \leq 4$), all bit APPs come from the channel decoder; otherwise, b_1 APPs come from the decoder and $b-b_1$ bit APPs come from the demapper. Since all symbols and bits are assumed independent, it follows that

$$P(\boldsymbol{x}_m|\boldsymbol{r}) = \prod_{l=0}^{\ell-1} P(x_{m\ell-l}|\boldsymbol{r})$$

where

$$P(x_{m\ell-l}|\boldsymbol{r}) = \prod_{h=1}^{b} P(c_{m\ell-l}^{(h)}|\boldsymbol{r}) \simeq \prod_{h=1}^{b} \frac{e^{\left(1-c_{m\ell-l}^{(h)}\right)\hat{\mathscr{L}}_{m\ell-l}^{(h)}}}{1+e^{\hat{\mathscr{L}}_{m\ell-l}^{(h)}}}$$

and

$$\mathscr{L}_{m\ell-l}^{(h)} \triangleq \ln \frac{P(c_{m\ell-l}^{(h)}=0|\boldsymbol{r})}{P(c_{m\ell-l}^{(h)}=1|\boldsymbol{r})}. \tag{4.20}$$

The LLRs $\{\mathscr{L}_{m\ell-l}^{(h)}\}$ are obtained from the channel decoder ($h \leq b_1$) or from the demapper ($b_1 < h \leq b$). If a given symbol $\tilde{x}^{(m_1)}$ has probability close to 1 at time instant $m\ell-l$, then $\alpha_{m\ell-l} \simeq \tilde{x}^{(m_1)}$. In particular, $\alpha_{m\ell-l} = P_{m\ell-l}$ if $P_{m\ell-l}$ is a pilot symbol.

4.3.2 Sliding Window

The BW strategy outlined in Section 4.3.1 relies on disjoint consecutive ℓ-symbol windows. A possible extension leads to the use of an ℓ-symbol sliding window, in which the phases estimated for a block of observable (on both polarizations) of length ℓ will be associated to the symbols at the center of the block. Such extensions will

help to overcome the limitation of the constant phase assumption with an increase in computational complexity. Filtering can be used to further improve the estimated phases. Taking into account the definition (4.18) and (4.19), the phase estimate at the epoch k can be expressed:

$$\hat{\varphi}^{(1)}_{k,\mathrm{PLP}} = \arg\left[\sum_{i=-\ell+1}^{\ell-1} \pi_i \Phi^{APP_1}_{ml+i,l}\right] \tag{4.21}$$

$$\hat{\varphi}^{(2)}_{k,\mathrm{PLP}} = \arg\left[\sum_{i=-\ell+1}^{\ell-1} \pi_i \Phi^{APP_2}_{ml+i,l}\right] \tag{4.22}$$

where $\{\pi\}$ are proper weights. The phase estimation strategy (4.21) is a generalized (APP-based) instance of the Phasor Linear Prediction (PLP) approach to phase estimation proposed in [45]. In particular, in (4.21) the weighting coefficients $\{\pi\}$ have a triangular shape, this is intuitively pleasing, as this gives the highest weight (namely, ℓ) to the k-th observable (associated with the k-th symbol). For this reason, we refer to this phase estimation strategy as APP-based PLP.

4.4 Iterative Receiver Structure

At this point, we describe the overall iterative receiver structure shown in Figure 4.1.

4.4.1 Front End

The first operation to be performed at the receiver is channel equalization. Perfect equalization is considered, i.e., the signals received on the two polarizations are multiplied by the matrix

$$\boldsymbol{G} \triangleq \begin{bmatrix} g_{11} & g_{12} \\ g_{21} & g_{22} \end{bmatrix} = \boldsymbol{H}^{-1}.$$

The goal of the block denoted as "XPIC" is to minimize the XPI between the two orthogonal polarizations and relies on the use of techniques, such as those proposed in [3, 68, 69] to improve the radio-link of the XPD system. XPIC is needed due to the presence of non-negligible XPI at the cross-polar branch, which cannot be accurately

estimated (as described in Section 4.3) without proper pre-compensation setup. In this work, feed-forward XPIC based on stochastic gradient method is used to improve the performance of the polarization of interest [3, 68, 69].

After XPIC compensation, the phases in correspondence to a block of data symbols is pre-estimated by means of linear interpolation between the estimated phases associated with the two consecutive pilot symbols at the border of the data symbols. In our scenario, the pilot symbols are used on the polarization of interest, where pilot symbols are available at the receiver. Although in [41] the author has shown that, in general, the optimized use of pilot symbols requires, at the receiver, the application of a Wiener filter, in this work we consider a linear interpolator for minimizing the system delay [47]. In fact, the linear interpolator minimizes the system delay, since only one frame has to be buffered to derive a phase estimate for each information symbol between two consecutive pilot symbols.

In correspondence to the pilot symbols, the phase noise process is simply estimated as the difference between the phase of the received sample and the phase of the transmitted symbol x_k:

$$\hat{\theta}_k^{(i)} = \angle r_k''^{(i)} x_k^{(i)*} \qquad\qquad i \in \{1,2\}$$

where, $r_k''^{(i)}$ corresponds to pre-compensation carried out by the XPIC on received observable $\tilde{r}_k^{(i)}$ for i-th polarization. Note that this estimation is asymptotically exact at high SNR. The observable at the output of the interpolator for the i-th polarization, denoted as $r_k^{(i)}$, can be expressed as follows:

$$r_k^{(i)} = r_k''^{(i)} e^{-\hat{\theta}_{k,\text{int}}} = x_k''^{(i)} e^{\left(\theta_k''^{(i)} - \hat{\theta}_{k,\text{int}}\right)} + n_k'^{(i)}$$

where $e^{-\hat{\theta}_{k,\text{int}}}$ is the derotation introduced by the interpolator, $x_k''^{(i)}$ and $\theta_k''^{(i)}$ correspond to $r_k''^{(i)}$. The additive noise process $\{n_k'^{(i)}\}$ is still i.i.d. Gaussian. The new phase noise process $\{\theta_k''^{(i)} - \hat{\theta}_{k,\text{int}}\}$ can no longer be characterized by the same model of $\{\theta_k\}$, e.g., a Wiener model. However, the APP-based synchronization algorithms do not require any a priori statistical characterization of the phase noise and, therefore, can be applied directly.

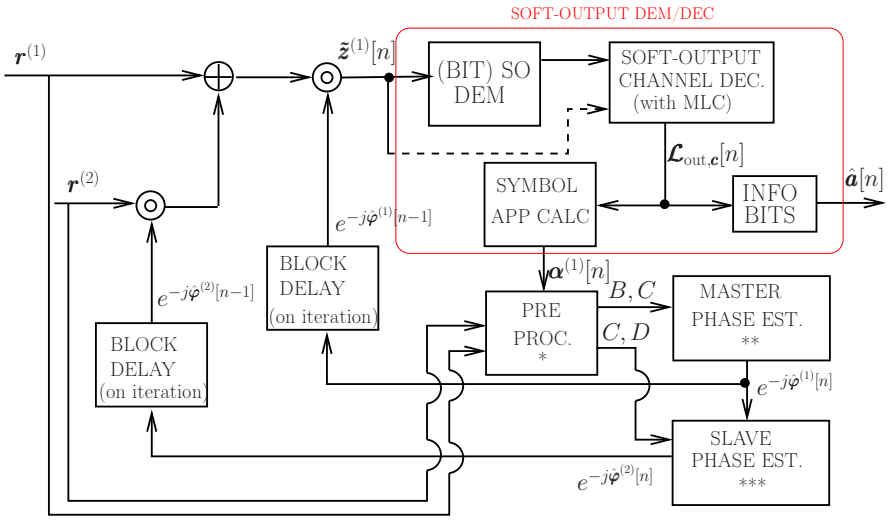

Figure 4.5: Block diagram of the iterative detection and synchronization.

This preliminary interference cancellation and phase estimation carried out by the FE are expedient to carry out the first decoding iteration, which is necessary to perform APP-based phase estimation and XPI cancellation. If FE compensation is not applied, even a mild phase noise can hinder the first decoding act, making following APP-based phase estimation and XPI cancellation ineffective.

4.4.2 Iterative Detection and Phase Estimation

Figure 4.5 shows the IDPE receiver for the MMSE-based phase estimation algorithm (4.9) derived in Section 4.3. As already anticipated, the receiver operates only on the polarization of interest and does not have access to data decided on the other polarization: this allows to have two completely independent modems on the two polarizations. The received observables at the output of the FE is used as reliable (bootstrap) input for the iterative synchronization receiver at its first iteration.

The other iterations will consider the observable $\{\boldsymbol{r}\}$ from both branches, which are fed directly to the input of the demodulator, whose soft-outputs are then passed to the soft-input soft-output decoder, which takes into account the presence of multi-

level coding (if required). The soft-output decoder generates LLRs on the (multi-level) coded bits, denoted as $\mathscr{L}_{\text{out},\boldsymbol{c}[\text{n}]}$, where n refers to the iteration number. In the presence of multi-level coding, the soft-output information associated with the free bits should be computed, according to the multi-level coding scheme in Section 4.2. The channel decoder provides soft output information on the coded bits and, therefore, one can compute the most likely code sequence $\hat{\boldsymbol{c}}$ output by the channel decoder. Since $b_1 = 4$, each length 4-bit substring $\{\hat{c}^{(b)}_{m\ell-l}\}_{b=1}^{4}$ identifies a subset $\mathscr{S}_{m\ell-l}$ associated with a (QAM) sub-constellation of size 2^{b_1}, corresponding to $b_1 = b-4$ free bits. At this point, one can compute the soft output on the free bits based on this sub-constellation. The LLRs on the channel coded bits and on the free bits can then be combined to generate APPs on the constellation symbols. The APPs then feed the phase estimator. We refer to a sequence of phase estimation and demodulation/decoding as an iteration.

The iterative algorithm can now be summarized as follows. We denote as n_{it} the maximum number of (external) iterations between demapper/decoder and phase estimator.[4] At the n-th iteration, the phase estimator operates on the following observable vector:

$$\tilde{\boldsymbol{z}}[n] = \left[\boldsymbol{r}^{(1)} + \boldsymbol{r}^{(2)} \circ e^{-\hat{\boldsymbol{\varphi}}^{(2)}[n-1]}\right] \circ e^{-\hat{\boldsymbol{\varphi}}^{(1)}[n-1]} \tag{4.23}$$

where $\boldsymbol{\varphi}[0] = 0$ and $\circ$ represents the Hadamard (or element-wise) product between two vectors. The vector $\tilde{\boldsymbol{z}}[n]$ has elements given by (4.8), where $\hat{\varphi}^{(1)}$ and $\hat{\varphi}^{(2)}$ can be derived from the (4.9) as explained in the Section 4.3. Note that, since the "clean" (after XPI cancellation and derotation) observable $\tilde{\boldsymbol{z}}[n]$ is used, the estimated phase corresponds to a residual phase error $\hat{\boldsymbol{\vartheta}}[n]$ to be used in the following iteration. The phase estimate, to be used in (4.23), is then updated as

$$\hat{\boldsymbol{\varphi}}[n] = \hat{\boldsymbol{\varphi}}[n-1] + \hat{\boldsymbol{\vartheta}}[n]. \tag{4.24}$$

After n_{it} iterations, a final decision on the transmitted bits $\hat{\boldsymbol{a}}$ is made.

The proposed algorithm and the corresponding receiver architecture in Figure 4.5 are inherently iterative, in the sense that at each iteration the decoding should be

[4] Note that external iteration refers to the number of iterations considered for phase estimation algorithm and in general different and independent from the detection iteration used for the decoder.

performed to obtain soft decisions to be fed at the input of the phase estimator.

4.5 Performance Analysis

In this section, we present simulation results for the considered receivers for different constellation sizes and phase noise intensities.

4.5.1 Simulation Setup

The XPD matrix $\boldsymbol{H}$ has elements

$$h_{ij} = \begin{cases} \frac{1}{\sqrt{1+\chi^2}} & \text{if } i = j; \quad i,j \in \{1,2\} \\ \frac{\chi}{\sqrt{1+\chi^2}} & \text{if } i \neq j; \quad i,j \in \{1,2\} \end{cases}$$

where the factor $1/\sqrt{1+\chi^2}$ is introduced for normalization purposes, so that the rows and columns of $\boldsymbol{H}$ have unitary energy. In the following, we consider $\chi = 10^{-\frac{15}{20}}$, i.e., the cross-polarization interference signal is 15 dB below the co-polar signal. Note that the channel XPD is large, i.e., there is good isolation between the orthogonal polarizations. Typically, channel XPD may vary between 15 dB and 5 dB: the largest value is associated with outdoor Line-of-Sight (LOS) scenario, whereas the smallest one is associated with scattering-rich Non-Line-of-Sight (NLOS) environments [70].

In all presented results, QAM is the considered modulation format and $N_{\mathrm{p}} = 1$ pilot symbol belongs to a 4-QAM constellation with average energy 2.5 times the average energy of data symbols is inserted in the frame every $N = 50$ symbols (unless otherwise stated). The channel code is an LDPC code with rate $R = k/n = 7/8$, with $k = 7056$ and $n = 8064$, unless otherwise stated. The exponent parity-check matrix construction (semi-random technique) and the encoding algorithm of the used LDPC code are those of the WiMAX standard [49, Paragraph 8.4.9.2.5, Annex H]. In particular, the exponent parity-check matrix has 12 rows, 96 columns, a spreading factor 84, a constant row weight 32 and an average column weight 4. LDPC decoding is based on the belief propagation algorithm.

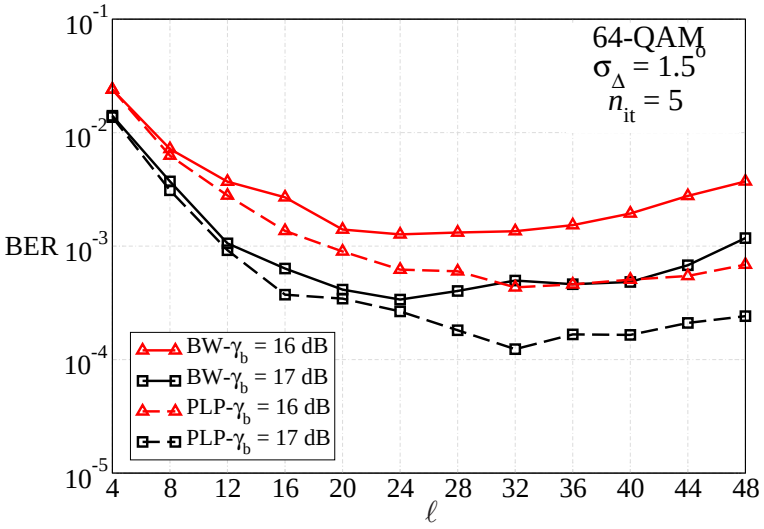

Figure 4.6: BER, as a function of ℓ, considering a 64-QAM, $n_{\text{it}} = 5$ iterations, and $\sigma_\Delta = 1.5^\circ$ for two different values of γ_b. Both BW and PLP phase estimation strategies are considered.

4.5.2 Numerical Results

The impact of the window length ℓ on the system performance is investigated in Figure 4.6. The BER is shown, as a function of ℓ, considering a scheme with 64-QAM, $n_{\text{it}} = 5$, $\sigma_\Delta = 1.5^\circ$, and various values of γ_b. Both BW and PLP phase estimation and XPI cancellation strategies are considered. The optimized window length is chosen as the one minimizing BER. In particular, $\ell = 24$ is a good window length with the BW strategy, for both considered values of γ_b. With the PLP strategy the performance improves, since the lowest achievable BER is lower than in the BW case. In general, $\ell = 32$ guarantees a good performance in all considered PLP cases. Moreover, our results suggest that the $\ell = 32$ is a good value for all considered constellation sizes and phase noise intensities, for both BW and PLP strategies.

In Figure 4.7, increasing the value of the number of iterations n_{it} improves the performance of the iterative receiver for both BW and PLP based phase noise estimation algorithms. Interestingly, the performance of the PLP approach at $n_{\text{it}} = 4$ is

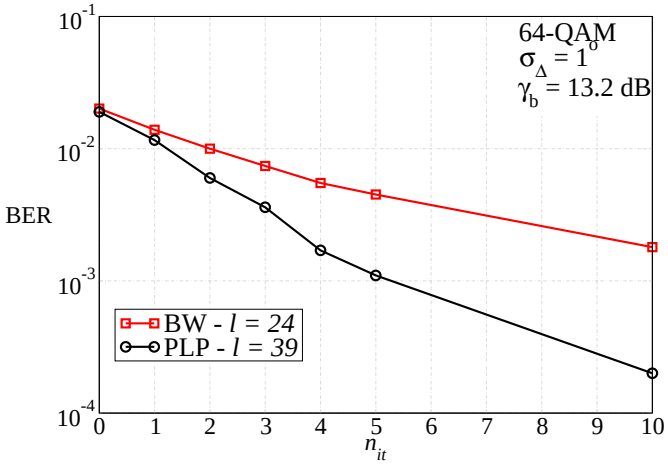

Figure 4.7: BER, as a function of n_{it}, considering a 64-QAM, different values of ℓ, and $\sigma_\Delta = 1^\circ$ for $\gamma_b = 13.2$ *dB*. Both BW and PLP phase estimation strategies are considered.

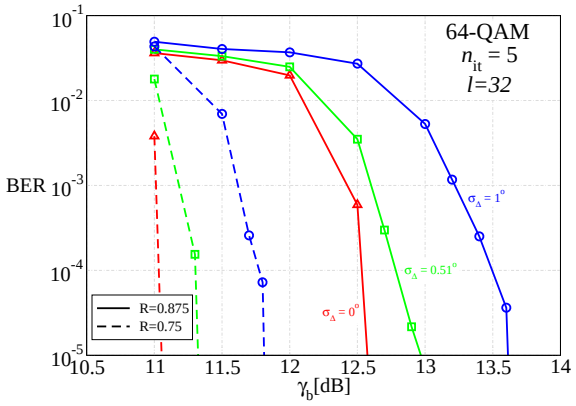

Figure 4.8: BER, as a function of γ_b, for various values of σ_Δ, considering $n_{\text{it}} = 5$ iterations, $\ell = 32$ with different coding rates R. Only PLP phase noise estimation strategy is considered.

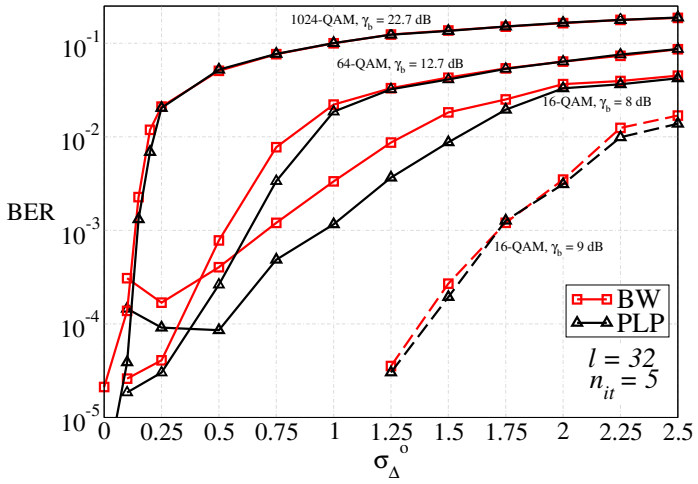

Figure 4.9: BER, as a function of σ_Δ, considering $n_{\text{it}} = 5$ iterations, $\ell = 32$, and various γ_b. The performance of BW and PLP are compared for (a) 16-QAM, (b) 64-QAM (c) 1024-QAM.

nearly equal to 10-th iteration of the BW approach, but this comes at the cost of a higher computational complexity.

As we know that the performance of the phase estimates rely on the APPs of the transmitted symbol. An increase in the coding rate would improve the performance of the proposed iterative synchronization receiver. Noticeable performance improvement can be seen in the Figure 4.8. Note that only PLP based phase estimation algorithm is used for comparison purpose.

In Figure 4.9, the BER is shown, as a function of σ_Δ, considering schemes with M-QAM (i.e., M = 16, 64, 1024), $n_{\text{it}} = 5$, iterations, $\ell = 32$, and various values of γ_b. Both BW and PLP strategies are considered. From Figure 4.9, it can be observed that the PLP approach is significantly better than the BW approach for low values of γ_b and σ_Δ. Both PLP and BW strategies have similar performance at higher values of σ_Δ.

From Figure 4.6 (and our preliminary analysis) for ℓ, we consider $\ell = 32$ to be a reasonable value for constellation of different sizes and different values of σ_Δ. In

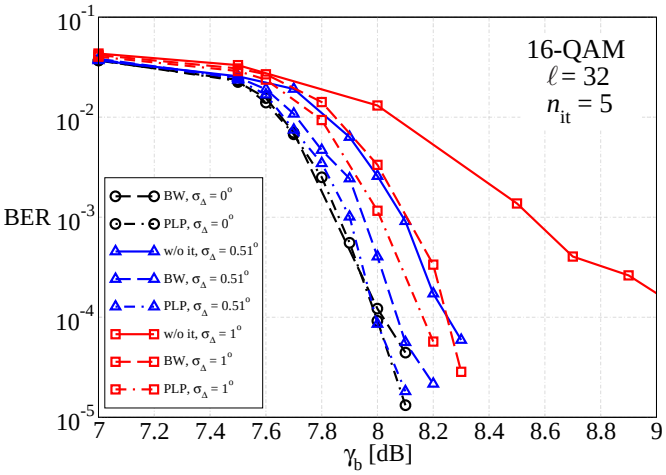

Figure 4.10: BER, as a function of γ_b, considering $n_{it} = 5$ iterations, $\ell = 32$, and various σ_Δ. The performance of BW and PLP are compared for 16-QAM.

Figure 4.10, the BER is shown, as a function of γ_b, considering $n_{it} = 5$ iterations, $\ell = 32$, and various values of σ_Δ. The performances of BW and PLP are compared for 16-QAM. As a reference, in Figure 4.10 we also show the performance without iterations (i.e., w/o it), i.e., in the case where, after FE processing, the demodulation and decoding are carried out only once. The case with $\sigma_\Delta = 0^\circ$ and $n_{it} = 5$ one corresponds to the performance of the XPD system in the absence of phase noise (i.e., idealized scenario), with both the FE and the IDPE blocks operational. We notice that the performance of the iterative receiver improves significantly using using IDPE sub-block. PLP approach performs better than the BW approach for different values of σ_Δ.

In Figure 4.11, the BER is shown, as a function of γ_b, considering $n_{it} = 5$ iterations, $\ell = 32$, and various values of σ_Δ. The performances of BW and PLP are compared for 1024-QAM. We remark that for high-order QAM (namely, 1024-QAM), the system has a detrimental performance without IDPE sub-block iterations. This is why no reference performance is shown in Figure 4.11. Also, multi-level coding is

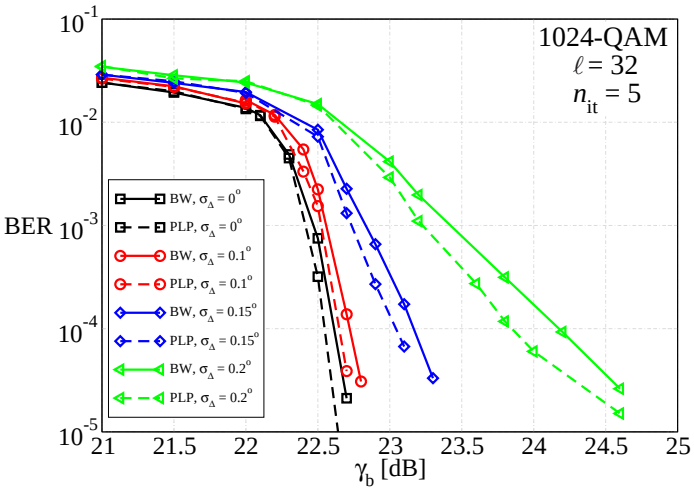

Figure 4.11: BER, as a function of γ_b, considering $n_{\text{it}} = 5$ iterations, $\ell = 32$, and various σ_Δ. The performance of BW and PLP are compared for 1024-QAM.

applied in the 1024-QAM case with $b_1 = 4$. For different values of σ_Δ, the performance of the PLP approach is better than the BW-based phase noise estimation.

The impact of the proposed phase estimation and XPI cancellation strategy embedded in the iterative receiver is evident, as the performance drastically improves using IDPE sub-block. Increasing the phase noise intensity degrades the performance, and this degradation is more pronounced for larger constellation sizes. However, for strong phase noise intensity the performance improvement brought by the PLP phase estimation and XPI cancellation strategy, with respect to the BW strategy, is significant, for both medium and high constellations.

4.6 Concluding Remarks

In the chapter, an innovative iterative synchronization receiver, which performs demodulation and decoding separately from the phase estimation process. In the phase estimation process, a novel Minimum Mean Square Error (MMSE)-based XPI can-

cellation algorithm is proposed.A system model has been derived for an XPD system in the presence of phase noise. The proposed iterative synchronization and decoding scheme integrates “off-the-shelf” blocks for demapping/decoding with separate MMSE-based phase estimation and XPI cancellation. The block-wise Master/Slave phase estimator with embedded XPI cancellation is used iteratively. The obtained results show that the proposed approach guarantees good performance for various constellation sizes, even for challenging phase noise-impaired scenarios.

Chapter 5

Conclusions

This chapter gives concluding remarks on the main results presented in this thesis. With the aim to have lower complexity, iterative phase synchronization receivers, which performs demodulation and decoding separately from the phase noise estimation process, have been proposed. Additionally, the proposed separate phase synchronization scheme has been employed for different channel impairments (such as: ISI and XPI). The obtained results show that this scheme allows tolerating high phase noise values for both small and medium-high constellations. We recall in the following, the main features of the designed scheme. The implementation complexity of the proposed scheme is kept lower by leaving unaltered the demapping/decoding operations, thus leading to the design of parallel iterative algorithms for phase synchronization having "off-the-shelf" blocks for different operations. The proposed phase noise estimation approach is also general, in the sense that it does not depend on (i) the considered modulation/coding scheme and (ii) the phase noise model, as it only exploits APPs of the transmitted (modulated) symbols generated by an "off-the-shelf" soft-output decoder. The proposed schemes leads to negligible performance degradation with respect to the ideal coherent system down to low signal-to-noise ratios, for both small and medium-high constellations.

In reduced complexity synchronization, a MAP-based algorithm is used to perform phase noise estimation. In particular, the algorithm uses APPs from the demap-

ping/decoding to perform phase synchronization. Different variants of APP-based phase noise estimation have been considered to improve the robustness of the iterative receiver. The proposed synchronization algorithms, in particular, the PLP approach guarantees a good performance for both small and medium-high constellations, even for challenging phase noise scenario. It was shown that the proposed algorithm has significantly lower complexity with respect to a joint-MAP based solution.

In the extended work, the separate synchronization and decoding algorithms are employed for channels impaired by ISI. A realistic continuous-time system model for an oversampled phase noise channel is derived. In the presence of an equivalent discrete-time system model, a low-complexity iterative synchronization and decoding receiver is devised, which exploits the received information from the channel by exchanging the information in an iterative fashion. With slight increase in the complexity, with respect to an equivalent traditional receiver, the proposed iterative receiver achieves better performance.

Finally, a system model has been derived for a dually-polarized system in the presence of phase noise. A separate APP-based synchronization and decoding strategy has been proposed. The proposed synchronization algorithm relies on an MMSE-based cancellation of the XPI followed by phase noise estimation on the polarization of interest. Two variants of MMSE-based phase noise estimation are considered: BW and PLP. The proposed iterative receiver operates only on the polarization of interest and has no access to the data decided on the other polarization, which allows to have two completely independent modems on both the polarizations. A comprehensive performance analysis has shown that the proposed iterative receiver is robust, for small-high order modulations, in the presence of strong phase noise.

Appendix A

Exchange of Sum-Product Operators

Let us denote, for the ease of simplicity, the term of the summation as

$$g(\boldsymbol{x}_k) \triangleq \prod_{l=0}^{\ell-1} p(r_{k-l}|\vartheta, x_{k-l}) P(x_{k-l}|\boldsymbol{r}) = \prod_{l=0}^{\ell-1} g_l(x_{k-l})$$

so that

$$\sum_{\boldsymbol{x}_k \in \mathscr{X}^\ell} \prod_{l=0}^{\ell-1} p(r_{k-l}|\vartheta, x_{k-l}) P(x_{k-l}|\boldsymbol{r}) = \sum_{\boldsymbol{x}_k \in \mathscr{X}^\ell} g(\boldsymbol{x}_k).$$

At this point, one can factor out the first term of the vector $\boldsymbol{x}_k$, thus obtaining

$$\sum_{\boldsymbol{x}_k \in \mathscr{X}^\ell} g(\boldsymbol{x}_k) = \sum_{x_k \in \mathscr{X}} g_0(x_k) \sum_{\boldsymbol{x}'_k \in \mathscr{X}^{\ell-1}} g'(\boldsymbol{x}'_k)$$

where $\boldsymbol{x}'_k$ is the $(\ell-1)$-length vector obtained by eliminating x_k from $\boldsymbol{x}_k$. One can recursively apply this approach, obtaining:

$$\sum_{\boldsymbol{x}_k \in \mathscr{X}^\ell} g(\boldsymbol{x}_k) = \sum_{x_k \in \mathscr{X}} g_0(x_k) \sum_{x_{k-1} \in \mathscr{X}} g_1(x_{k-1}) \cdots \sum_{x_{k-\ell} \in \mathscr{X}} g_{\ell-1}(x_{k-\ell}) = \prod_{l=0}^{\ell-1} \sum_{x \in \mathscr{X}} g_l(x)$$

where, in the last step, we have used the fact that the symbols $\{x_{k-l}\}$ $(l = 0, \ldots, \ell-1)$ are all QAM symbols in the same alphabet $\mathscr{X}$.

Bibliography

[1] J. Rutman and FL Walls. Characterization of frequency stability in precision frequency sources. *Proc. IEEE*, 79(7):952–960, July 1991.

[2] R.U. Nabar, H. Bolcskei, V. Erceg, D. Gesbert, and A.J. Paulraj. Performance of multiantenna signaling techniques in the presence of polarization diversity. *IEEE Trans. Signal Processing*, 50(10):2553–2562, Oct 2002. doi:10.1109/TSP.2002.803322.

[3] R. Raheli and G. Picchi. Synchronous and fractionally-spaced blind equalization in dually-polarized digital radio links. In *Proc. IEEE Intern. Conf. on Commun.* (ICC), volume 1, pages 156–161, Denver, CO, USA, June 1991.

[4] L. Tomba. On the effect of wiener phase noise in ofdm systems. *IEEE Trans. Commun.*, 46(5):580–583, May 1998. doi:10.1109/26.668721.

[5] S. Suyama, H. Suzuki, K. Fukawa, and J. Izumi. Iterative receiver employing phase noise compensation and channel estimation for millimeter-wave ofdm systems. *IEEE J. Select. Areas Commun.*, 27(8):1358–1366, October 2009. doi:10.1109/JSAC.2009.091006.

[6] H. Mehrpouyan, A.A. Nasir, S.D. Blostein, T. Eriksson, G.K. Karagiannidis, and T. Svensson. Joint estimation of channel and oscillator phase noise in mimo systems. *IEEE Trans. Signal Processing*, 60(9):4790–4807, Sept 2012. doi:10.1109/TSP.2012.2202652.

[7] A. Tarable, G. Montorsi, S. Benedetto, and S. Chinnici. An EM-based phase-noise estimator for MIMO systems. In *Proc. IEEE Intern. Conf. on Commun.* (ICC), pages 3215–3219, Budapest, Hungary, June 2013.

[8] G Durisi, A. Tarable, C. Camarda, R. Devassy, and G. Montorsi. Capacity bounds for mimo microwave backhaul links affected by phase noise. *IEEE Trans. Commun.*, 62(3):920–929, March 2014.

[9] A. Barbieri and G. Colavolpe. On the information rate and repeat-accumulate code design for phase noise channels. *IEEE Trans. Commun.*, 59(12):3223–3228, December 2011.

[10] L. Barletta, M. Magarini, and A. Spalvieri. The information rate transferred through the discrete-time Wiener's phase noise channel. *J. Lightwave Technol.*, 30(10):1480–1486, May 2012.

[11] M. Martalò, C. Tripodi, and R. Raheli. On the information rate of phase noise-limited communications. In *Information Theory and Applications Workshop* (ITA), pages 1–7, San Diego, CA, USA, February 2013.

[12] H. Ghozlan and G. Kramer. Multi-sample receivers increase information rates for Wiener phase noise channels. In *Proc. IEEE Global Telecommun. Conf.* (GLOBECOM), pages 1897–1902, December 2013.

[13] J. G. Proakis. *Digital Communications, 4th Ed.* McGraw-Hill, New York, NY, USA, 2001.

[14] U. Mengali and A. DÁndrea. Synchronization techniques for digital receivers. *Plenum Press*, 1997.

[15] M. Moeneclaey H.Meyr and S. Fechtel. Digital communication receivers: Synchronization, channel estimation and and signal processing. *John Wiley & Sons*, 1998.

[16] F. M. Gardner. *Phaselock Techniques*. John Wiley & Sons, New York, NY, USA, 1979.

[17] C. Berrou, A. Glavieux, and P. Thitimajshima. Near shannon limit error-correcting coding and decoding: Turbo-codes. 1. In *Proc. IEEE Intern. Conf. on Commun.* (ICC), volume 2, pages 1064–1070, May 1993. doi:10.1109/ICC.1993.397441.

[18] R. G. Gallager. Low density parity check codes. *IEEE Trans. Inform. Theory*, 8(1):21–28, January 1962.

[19] C. Herzet, N. Noels, V. Lottici, H. Wymeersch, M. Luise, M. Moeneclaey, and L. Vandendorpe. Code-aided turbo synchronization. *Proc. IEEE*, 95(6):1255–1271, June 2007.

[20] N. Noels, H. Steendam, and M. Moeneclaey. Performance analysis of ML-based feedback carrier phase synchronizers for coded signals. *IEEE Trans. Signal Processing*, 55(3):1129–1136, March 2007.

[21] M. Nissila and S. Pasupathy. Adaptive iterative detectors for phase-uncertain channels via variational bounding. *IEEE Trans. Commun.*, 57(3):716–725, March 2009.

[22] L. Benvenuto, L. Giugno, V. Lottici, and M. Luise. Code-aware carrier phase noise compensation on turbo-coded spectrally-efficient high-order modulations. In *Proc. Int. Workshop Signal Processing for Space Communications* (SPSC), pages 1–8, Catania, Italy, September 2003.

[23] Jabran Bhatti and Marc Moeneclaey. Feedforward data-aided phase noise estimation from a dct basis expansion. *EURASIP Journal on Wireless Communications and Networking*, 2009(1):568570, 2009. URL: http://jwcn.eurasipjournals.com/content/2009/1/568570, doi:10.1155/2009/568570.

[24] J. Bhatti and M. Moeneclaey. Iterative soft-decision-directed phase noise estimation from a dct basis expansion. In *Personal, Indoor and Mobile Radio Communications, 2009 IEEE 20th International Symposium on*, pages 3228–3232, Sept 2009. doi:10.1109/PIMRC.2009.5450119.

[25] N. Noels, J.Bhatti, H.Bruneel, and M.Moeneclaey. Block-processing soft-input soft-output demodulator for coded psk using dct-based phase noise estimation. *IEEE Trans. Commun.*, 62(8):2939–2950, Aug 2014. doi:10.1109/TCOMM.2014.2338871.

[26] Liang Zhao and Won Namgoong. A novel phase-noise compensation scheme for communication receivers. *IEEE Trans. Commun.*, 54(3):532–542, March 2006. doi:10.1109/TCOMM.2006.869788.

[27] V. Simon, A. Senst, M. Speth, and H. Meyr. Phase noise estimation via adapted interpolation. In *Proc. IEEE Global Telecommun. Conf.* (GLOBECOM), volume 6, pages 3297–3301 vol.6, 2001. doi:10.1109/GLOCOM.2001.966296.

[28] E. Ip and J. M. Kahn. Feedforward carrier recovery for coherent optical communications. *J. Lightwave Technol.*, 25(9):2675–2692, September 2007.

[29] N. Kamiya and E. Sasaki. Pilot-symbol assisted and code-aided phase error estimation for high-order qam transmission. *IEEE Trans. Commun.*, 61(10):4369–4380, October 2013. doi:10.1109/TCOMM.2013.090213.120763.

[30] S.Pecorino, S. Mandelli, L.Barletta, M.Magarini, and A.Spalvieri. Bootstrapping iterative demodulation and decoding without pilot symbols. *J. Lightwave Technol.*, 33(17):3613–3622, Sept 2015. doi:10.1109/JLT.2015.2448109.

[31] G. Ferrari, A. Anastasopoulos, G. Colavolpe, and R. Rahel. Adaptive iterative detection for the phase-uncertain channel: limited-tree-search versus truncated-memory detection. *IEEE Trans. Veh. Technol.*, 53(2):433–442, March 2004. doi:10.1109/TVT.2004.823532.

[32] C. Herzet, N. Noels, V. Lottici, H. Wymeersch, M. Luise, M. Moeneclaey, and L. Vandendorpe. Code-aided turbo synchronization. *Proc. IEEE*, 95(6):1255–1271, June 2007. doi:10.1109/JPROC.2007.896518.

[33] G. Colavolpe, A. Barbieri, and G. Caire. Algorithms for iterative decoding in the presence of strong phase noise. *IEEE J. Select. Areas Commun.*, 23(9):1748–1757, Sept 2005. doi:10.1109/JSAC.2005.853813.

[34] P. Andrew Worthen and W.E. Stark. Unified design of iterative receivers using factor graphs. *IEEE Trans. Inform. Theory*, 47(2):843–849, Feb 2001. doi:10.1109/18.910595.

[35] J. Dauwels and H.-A. Loeliger. Phase estimation by message passing. In *Proc. IEEE Intern. Conf. on Commun.* (ICC), volume 1, pages 523–527 Vol.1, June 2004. doi:10.1109/ICC.2004.1312544.

[36] S. Shayovitz and D. Raphaeli. Message passing algorithms for phase noise tracking using tikhonov mixtures. *IEEE Trans. Commun.*, PP(99):1–15, 2015. doi:10.1109/TCOMM.2015.2506553.

[37] U. Wachsmann, R. F. H. Fischer, and J. B. Huber. Multilevel codes: theoretical concepts and practical design rules. *IEEE Trans. Inform. Theory*, 45(5):1361–1391, July 1999.

[38] G. Ungerboeck. Channel coding with multilevel/phase signals. *IEEE Trans. Inform. Theory*, 28:55–67, January 1982.

[39] Y. Li and W. E. Ryan. Bit-reliability mapping in LDPC-coded modulation systems. *IEEE Commun. Lett.*, 9(1):1–3, January 2005.

[40] R. D. Wesel, X. Liu, J. M. Cioffi, and C. Komninakis. Constellation labeling for linear encoders. *IEEE Trans. Inform. Theory*, 47(6):2417–2431, September 2001.

[41] J. K. Cavers. An analysis of pilot symbol assisted modulation for rayleigh fading channels. *IEEE Trans. Veh. Technol.*, 40(4):686–693, 1991.

[42] A. Demir, A. Mehrotra, and J. Roychowdhury. Phase noise in oscillators: a unifying theory and numerical methods for characterization. *IEEE Tran. Circuits*

and Systems I: Fundamental Theory and Applications, 47(5):655–674, May 2000.

[43] D. Petrovic, W. Rave, and G. Fettweis. Effects of phase noise on ofdm systems with and without pll: Characterization and compensation. *IEEE Trans. Commun.*, 55(8):1607–1616, Aug 2007. doi:10.1109/TCOMM.2007.902593.

[44] V. Lottici and M. Luise. Embedding carrier phase recovery into iterative decoding of turbo-coded linear modulations. *IEEE Trans. Commun.*, 52(4):661–669, April 2004.

[45] G. Ferrari, G. Colavolpe, and R. Raheli. On linear predictive detection for communications with phase noise and frequency offset. *IEEE Trans. Veh. Technol.*, 56(4):2073–2085, July 2007.

[46] R. Schober and W. H. Gerstacker. Metric for noncoherent sequence estimation. *IEE Electronics Letters*, 35(25):2178–2179, December 1999.

[47] J. M. Torrance and L. Hanzo. Comparative study of pilot symbol assisted modem schemes. In *Proc. Int. Conf. Radio Receivers and Associated Systems*, pages 36–41, Bath, UK, September 1995.

[48] A. Barbieri, G. Colavolpe, and G. Caire. Joint iterative detection and decoding in the presence of phase noise and frequency offset. *IEEE Trans. Commun.*, 55(1):171–179, January 2007.

[49] Approved Draft IEEE Standard for Local and metropolitan area networks Corrigendum to IEEE Standard for Local and Metropolitan Area Networks-Part 16: Air Interface for Fixed Broadband Wireless Access Systems (Incorporated into IEEE Std 802.16e-2005 and IEEE Std 802.16-2004/Cor 1-2005 E). *IEEE Std P802.16/Cor1/D5*, 2005.

[50] S. Shayovitz and D. Raphaeli. Efficient iterative decoding of LDPC in the presence of strong phase noise. In *Proc. Intern. Symp. on Turbo Codes & Relat. Topics*, pages 1–5, Gothenburg, Sweden, August 2012.

[51] M. Martalò, G. Ferrari, M. Asim, J. Gambini, C. Mazzucco, G. Cannalire, S. Bianchi, and R. Raheli. Reduced-complexity synchronization for high-order coded modulations. In *Proc. IEEE Intern. Conf. on Commun.* (ICC), June 2015.

[52] M.R. Khanzadi, D. Kuylenstierna, A. Panahi, T. Eriksson, and H. Zirath. Calculation of the performance of communication systems from measured oscillator phase noise. *IEEE Transactions on Circuits and Systems I: Regular Papers*, 61(5):1553–1565, May 2014. doi:10.1109/TCSI.2013.2285698.

[53] M. Martalò, A. Gervasi, C. Tripodi, and R. Raheli. Information rate analysis of the oversampled phase-noise channel. In *2015 12th International Symposium on Wireless Communications Systems (ISWCS)*, Aug 2015. doi:10.1109/ISWCS.2014.6933363.

[54] L. Ros J. Vila` Valls and J. M. Brossier. Joint oversampled carrier and time-delay synchronization in digital communications with large excess bandwidth. *ELSEVIER Signal Processing*, 92(01):76 –88, 2012.

[55] F. Septier, Y. Delignon, A. Menhaj-Rivenq, and C. Garnier. Particle filter with hybrid importance function for joint symbol detection and phase tracking. In *IEEE 7th Workshop on Signal Processing Advances in Wireless Communications, 2006. SPAWC '06.*, pages 1–5, July 2006. doi:10.1109/SPAWC.2006.346358.

[56] Zhixiang Shen, Hongyi Yu, Yunpeng Hu, and Caiyao Shen. Joint symbol detection for multi-receiver without signal synchronization and array alignment. *IEEE Commun. Lett.*, 18(10):1755–1758, Oct 2014. doi:10.1109/LCOMM.2014.2352644.

[57] O. Ozdemir, Ruoyu Li, and P.K. Varshney. Hybrid maximum likelihood modulation classification using multiple radios. *IEEE Commun. Lett.*, 17(10):1889–1892, October 2013. doi:10.1109/LCOMM.2013.081913.131351.

[58] D. Fertonani, A. Barbieri, and G. Colavolpe. Reduced-complexity bcjr algorithm for turbo equalization. *IEEE Trans. Commun.*, 55(12):2279–2287, Dec 2007. doi:10.1109/TCOMM.2007.910638.

[59] B.L. Yeap, Choong Hin Wong, and L. Hanzo. Reduced complexity in-phase/quadrature-phase m-qam turbo equalization using iterative channel estimation. *IEEE Trans. Wireless Commun.*, 2(1):2–10, Jan 2003. doi:10.1109/TWC.2002.806355.

[60] G. Ferrari, G. Colavolpe, and R. Raheli. On trellis-based truncated-memory detection. *IEEE Trans. Commun.*, 53(9):1462–1476, Sept 2005. doi:10.1109/TCOMM.2005.855008.

[61] Yuxin Cheng Haige Xiang Lei Zhang, Yong Shang. Improved turbo equalization based on soft isi cancellation. *ELSEVIER Signal Processing*, 89:1812–1820, 2009.

[62] M. TuÌĹchler, A.C. Singer, and R. Koetter. Minimum mean squared error equalization using a priori information. *IEEE Trans. Signal Processing*, 50(3):673–683, Mar 2002. doi:10.1109/78.984761.

[63] H. Meyr, M. Oerder, and A. Polydoros. On sampling rate, analog prefiltering, and sufficient statistics for digital receivers. *IEEE Trans. Commun.*, 42(12):3208–3214, Dec 1994. doi:10.1109/26.339842.

[64] Piero Castoldi and Riccardo Raheli. On recursive optimal detection of linear modulations in the presence of random fading. *European Transactions on Telecommunications*, 9(2):209–220, 1998.

[65] Lukas Landau, Stefan Krone, and Gerhard Fettweis. Intersymbol-interference design for maximum information rates with 1-bit quantization and oversampling at the receiver. In *9th International ITG Conference on Systems, Communication and Coding (SCC), Proceedings of 2013*, pages 1–6, Jan 2013.

[66] L. Landau and G. Fettweis. Information rates employing 1-bit quantization and oversampling at the receiver. In *2014 IEEE 15th International Workshop on Signal Processing Advances in Wireless Communications (SPAWC)*, pages 219–223, June 2014. doi:10.1109/SPAWC.2014.6941477.

[67] F. Vogelbruch and Sven Haar. Low complexity turbo equalization based on soft feedback interference cancellation. *IEEE Commun. Lett.*, 9(7):586–588, July 2005. doi:10.1109/LCOMM.2005.1461672.

[68] A. Eliaz, A. Turgeman, A. Aharony, and J. Friedmann. Modem control using cross-polarization interference estimation, November 2009. US Patent No. 7613260.

[69] L. Popken, W. Kriedte, O. Bender, and M. Luise. Synchronization failure rates in master-slave synchronized phase-locked loops. *IEEE Trans. Aerosp. Electron. Syst.*, 29(2):328–335, Apr 1993. doi:10.1109/7.210071.

[70] H. Asplund, J. E Berg, F. Harrysson, J. Medbo, and M. Riback. Propagation characteristics of polarized radio waves in cellular communications. In *Proc. IEEE Vehicular Tech. Conf.* (VTC), pages 839–843, Sept 2007. doi:10.1109/VETECF.2007.184.

Acknowlegment

Many people helped me during these years as a Ph.D. student, and it is now time to thank them. I would like to begin by expressing my sincere gratitude towards my advisor and mentor, Prof. Gianluigi Ferrari for his valuable guidance and advice throughout my research at the Wireless Ad-hoc Sensor Network (WASN) lab, Department of Information Engineering, University of Parma. Special thanks to my tutor, Dr. Marco Martalò for the opportunity to pursue research under his tutelage. His enthusiasm, discussions, and guidance were of greater help in the realization of this thesis. I am thankful to all faculty members of the department, who are always supportive and helpful in understanding and enhancing my knowledge.

Thanks to all my lab-mates and fellow students at the department, for their support and guidance in different matters, throughout my stay. I am also thankful to my family members for their utmost encouragement and support. Finally, I would like to acknowledge the financial support from the department for my research activities and other expenditure.